Osaka University Knowledge Archive

Title	Piezo1 Mutant Zebrafish as a Model of Idiopathic Scoliosis
Author(s)	Ramli
Citation	大阪大学, 2024, 博士論文
Version Type	VoR
URL	https://doi.org/10.18910/96343
rights	
Note	

Osaka University Knowledge Archive : OUKA

https://ir.library.osaka-u.ac.jp/

Osaka University

Piezo1 Mutant Zebrafish as a Model of Idiopathic Scoliosis

Ramli

Laboratory of Pattern Formation
Graduate School of Frontier Biosciences
Osaka University

A thesis submitted
for the degree of Doctor of Philosophy of Science
March 2024

Abstract

Scoliosis is a condition where the spine curves sideways, unique to humans due to their upright posture. However, the cause of this disease is not well understood because it's challenging to find a model for experimentation. This study aimed to create a model for human idiopathic scoliosis by manipulating the function of mechanosensitive channels called Piezo channels in zebrafish. Zebrafish were chosen because they experience similar biomechanical forces to humans, particularly in relation to the role of mechanical force in scoliosis progression.

At first, I identified that zebrafish have 3 different of piezo genes; *piezo1, piezo2a,* and *piezo2b*. Although *piezo1* and *piezo2a* are not paralog genes, the expression pattern is almost similar which broadly expressed throughout the body. While *piezo2b* is concentrated in neuron cell. With this information, I assumed that *piezo1* and *piezo2a* might have overlapping function and might involve in bone formation.

As I expected from the similarity of expression pattern, the single mutants of *piezo1*$^{-/-}$ and *piezo2a*$^{-/-}$ were viable and fertile. Neither mutant showed morphological abnormalities in the larval and juvenile stages, and can survive until adult. Interestingly, double knock out of *piezo1* and *piezo2a* resulting in congenital systemic malformations with the lack of mineralization and died after 10 days. This suggest that *piezo1* and *piezo2a* have redundant function in bone formation.

To avoid lethality, piezo1 in-frame mutation was generated, targeting splice acceptor sequence of exon 2 resulting 11 amino acid deletions of *piezo1* coding sequences. Although, did not alter reading frame, the channel activity was significantly decrease. Phenotypically, an in-frame mutation of *piezo1* led to fully penetrant juvenile-onset scoliosis, bone asymmetry, reduced tissue mineral density, and progressive vertebral column—resembling non-congenital scoliosis symptoms in humans. In addition, I also confirmed that abnormal osteoblast function might be the causative factor of this phenotype.

In conclusion, these findings suggest that functional Piezo channels responding to mechanical forces are crucial for bone formation and maintaining spine integrity, providing insights into skeletal disorders. Moreover, this mutant mimic human idiopathic scoliosis and can be used for disease model.

Content

Abstract **2**
Content **3**
1. Introduction **5**
1.1 Vertebral Bone 5
1.1.1 Development of vertebral bone 5
1.1.2 Vertebral bone stability 6
1.2 Scoliosis 7
1.2.1 Type of scoliosis 7
1.2.2 Factors that contribute in the development of idiopathic scoliosis 8
1.3 Mechanical force and scoliosis 8
1.4 Animal model for studying scoliosis 9
1.4.1 Mice and chick 9
1.4.2 Zebrafish 10
1.5 Piezo channel as a Mechanoreceptor 11
1.5.1 General properties of Piezo channels. 11
1.5.2 Activation mechanism 12
1.5.3 Bone, mechanical forces, and Piezo channel 13
1.6 Piezo channel and scoliosis 14
1.7 Thesis overview 15
2. Material and Method **16**
2.1 Zebrafish Husbandry 16
2.2 Generation *piezo1* and *piezo2a* Knockout zebrafish by CRISPR/Cas9 system 16
2.3 Generation *piezo1* in-frame mutant zebrafish by CRISPR/Cas9 system 17
2.4 Microinjection and genotyping 17
2.5 Micro-CT 17
2.6 Alizarin Red S staining 18
2.7 Histology and Alkaline Phosphatase staining 18
2.8 RNA extraction and cDNA synthesis 18
2.9 Cell-attached patch clamp mode 18
2.10 qPCR 18
2.11 Rescue experiment with introducing functional *piezo1* 19
2.12 Statistical analysis 19
3. Results **20**

3.1 Generation of piezo null mutant 20
3.2 Phenotypes of the zebrafish with double mutations of *piezo1* and *piezo2a* 20
3.3 Mosaic mutant displays bone curvature 25
3.4 Generation of *piezo1* in-frame mutant 25
3.5 *piezo1* in-frame mutant (*piezo1*$^{11aa\ del/11aa\ del}$) develops juvenile-onset scoliosis 27
3.6 Detailed observation of vertebra shape by micro-CT 27
3.7 Abnormal osteoblast function 30
3.8 Progressive abnormalities in vertebral column of *piezo1*$^{11aa\ del/11aa\ del}$ 30
3.9 Introducing functional *piezo1* gene into *piezo1* scoliosis mutant could develop normal spine 33
3.10 Increase muscle mass could alleviate scoliosis symptoms 33
4. Discussion and Conclusion 37
4.1 Usefulness as a pathological model 38
4.2 Causal relationship between scoliosis and osteoporosis 38
4.3 *piezo1* and *piezo2a* might have overlapping function 40
4.4 *piezo1*$^{11aa\ del/11aa\ del}$ mutant for a tool to investigate the *piezo* genes in other cells 40
Bibliography 41
Achievement 47

Chapter 1

1. Introduction

1.1 Vertebral Bone

The vertebral column, commonly known as the backbone or spine, serves as a crucial support for the body and provides protection to the spinal cord. Comprising a series of vertebral bones connected by intervertebral discs, these bones exhibit variations in size and shape. Typically, a vertebra consists of two main parts: the vertebral body, positioned anteriorly, and the vertebral arches, located posteriorly (Figure 1.1). Vertebral body progressively increases in size and thickness to bear the body weight. On the other hand, the vertebral arches enclose the vertebral foramen, housing the spinal cord. Constructed from laminae, transverse processes, and spinous processes, the vertebral arches collectively form the posterior aspect of the spine (Turnquist & Minugh-Purvis, 2012).

Meanwhile, the intervertebral disc, characterized by its fibrocartilaginous nature, functions as a cushion between vertebrae during weight-bearing activities. This explains the thinner profile of intervertebral discs in the cervical region compared to the lumbar region. The disc comprises two essential components, namely the annulus fibrosus and the nucleus pulposus, both of which play a crucial role in managing mechanical stress within the spine (Crispino &Crispino, 2015).

1.1.1 Development of vertebral bone

The vertebral column takes shape during embryogenesis through the rhythmic development of somites from the anterior to posterior regions. Each somite undergoes differentiation into three main components: the sclerotome, contributing to the skeleton and cartilage; the dermatome, forming the dermis; and the myotome, developing into muscle. By the fourth week of gestation, sclerotomal cells migrate in three directions. 1) Some cells move ventro-medially around the notochord to give rise to the vertebral body. 2) Others migrate dorsally behind the neural tube, enveloping the developing spinal cord to form the vertebral arch. 3) The remaining cells pass ventro-laterally, contributing to the coastal element of vertebrae, eventually developing into ribs in the thoracic regions (Figure 1.2) (Scaal, 2016).

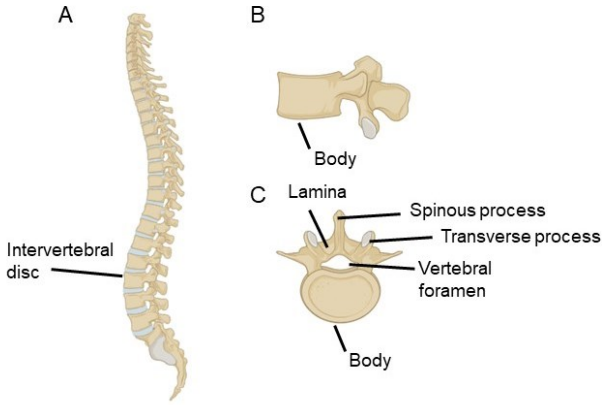

Figure 1.1 General structure of vertebral bone. (A) Overview of vertebral column. (B) Lateral view of single vertebrae. (C) Superior view of single vertebrae

The development of vertebrae progresses through three stages: the mesenchymal stage, chondrification stage, and ossification stage. During the mesenchymal stage, occurring between the 4th and 6th weeks of gestation, mesenchymal cells, particularly in the sclerotome, surround the developing notochord and migrate in three directions as previously described. Following this, chondrification centers, responsible for producing cartilage, emerge after the 6th week, with two centers forming in each half of the centrum. These centers eventually merge into a solid block of cartilage. Concurrently, ossification centers develop within the cartilaginous model, initiating the process of endochondral ossification, which involves the replacement of cartilage with bone tissue. These ossification centers are crucial in marking the onset of bone formation and differentiate into various components of the vertebrae, such as the vertebral body, neural arches, and processes, collectively contributing to the formation of mature vertebral bones (Scaal, 2016).

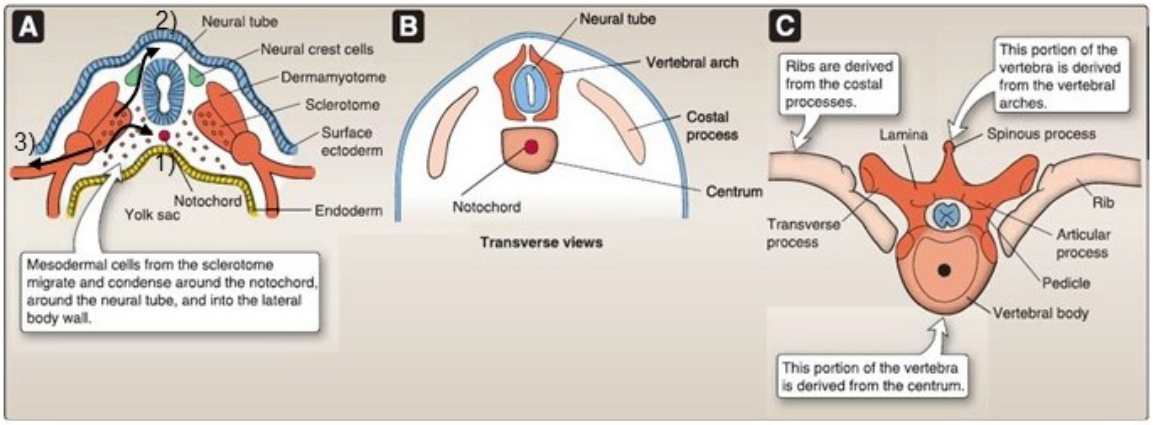

Figure 1.2 Early development of vertebral bone. (A) At 28 days, mesodermal cell from sclerotome migrate and condense in three different areas; around notochord to develop vertebral body, around neural tube to rise vertebral arches, and into lateral side to develop transverse process and ribs. (B) Development of centrum, arches and coastal processes. (C) structure of vertebrae in adult stage (Harrel & Dudek, 2019) .

1.1.2 Vertebral bone stability

Spinal stability refers to the capacity of the spinal column to uphold its form when subjected to typical physiological stresses, thereby averting any displacement. The preservation of spinal stability is crucial for preventing injuries, alleviating back pain, and facilitating bodily movements. This stability is upheld through the collaboration of three closely linked subsystems: the passive subsystem (comprising vertebrae, discs, and ligaments), the active subsystem (consisting of muscles and tendons), and the neural control subsystem (encompassing the nervous system) (Figure 1.3) (Panjabi, 1992).

Within the passive subsystem, the intrinsic functions of bone, discs, and ligaments play a relatively modest role in maintaining spinal stability. Additionally, this subsystem incorporates mechanoreceptors that transmit proprioceptive signals from the spine to the central nervous system. Conversely, the active subsystem, comprising muscles and tendons, plays a key role in ensuring stability, particularly during activities such as standing, lifting, and bending. The absence of muscular support would render the spine highly unstable, even under minimal loads. Lastly, the neural control subsystem integrates input from both the passive and active

subsystems and subsequently directs the muscles surrounding the spine to stabilize it (Studnicka & Ampat, 2023).

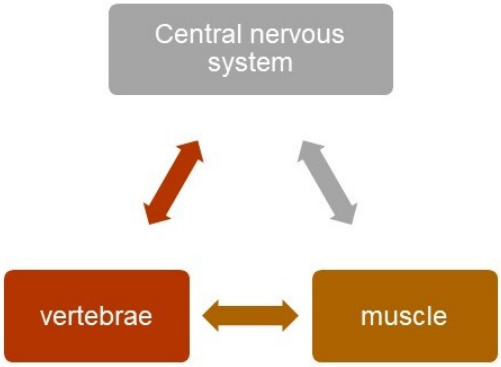

Figure 1.3 The stability of the spine is regulated by three interconnected subsystems: the spinal column, muscles, and central nervous system. If any of these subsystems experiences acute or chronic damage, the other components must compensate by engaging in additional work.

When the coordination among these elements is disrupted, it can lead to spinal instability, characterized by abnormal displacement within the motion segment under normal physiological loads. This condition may contribute to the advancement of scoliosis as one of its effects.

1.2 Scoliosis

Scoliosis is a medical condition characterized by an abnormal lateral curvature of the spine. The spine may take on an "S" or "C" shape when viewed from the back. This bone condition is common in children and adolescents, when massive body growth is occurred. The degree of spinal curvature in scoliosis is typically measured in degrees, and a curve of more than 10 degrees is generally considered diagnostic. In addition to the lateral curvature, scoliosis can involve vertebral rotation, where the vertebrae twist around the axis of the spine (Konieczny et al., 2013). It is estimated that approximately 5% of the global population is affected by scoliosis. Interestingly, when considering gender differences, females are more susceptible to developing scoliosis compared to males(Chung et al., 2020).

1.2.1 Type of scoliosis

Scoliosis can be classified into congenital, idiopathic, and neuromuscular types based on its causes. Congenital scoliosis results from vertebral malformation during embryonic development and can be detected at an early age, with malformations like hemivertebrae, unilateral bar, or block vertebrae. Two identified genes associated with congenital scoliosis are DLL3, which encodes the notch ligand delta-like 3, an inhibitor of the notch pathway, and JAG1, which encodes a ligand for the Notch transmembrane receptor crucial for development (Li et al., 1997;Bulman et al., 2000).

Neuromuscular scoliosis is attributed to abnormal muscle function around the spine, often linked to conditions like cerebral palsy, spinal muscular atrophy, or spinal cord injuries. Moreover, Idiopathic scoliosis, the most prevalent form, occurs during adolescence, and its exact mechanism remains unknown (Konieczny et al., 2013).

1.2.2 Factors that contribute in the development of idiopathic scoliosis

A study found that the pathogenesis of idiopathic scoliosis, particularly in young females, is linked to abnormalities in the central nervous system. The development of scoliosis in puberty among young women is attributed to the disharmony between two nervous systems: autonomic (*leptin-hypothalamic-sympathetic nervous system - LHS - concept*) and somatic (*escalator concept)* This imbalance, exacerbated by hormonal influences leading to systemic skeletal overgrowth, is proposed as the double neuro-osseous theory (Burwell et al., 2009).

Furthermore, a study conducted in 2015 demonstrated the involvement of hormonal imbalance in the onset of idiopathic scoliosis. The researchers assessed the levels of female hormones, including FSH, LH, estrogen, progesterone, as well as serum concentrations of RANKL and osteocalcin, in girls with idiopathic scoliosis and compared them with control groups. The findings revealed a significant decrease in female hormone levels in girls with scoliosis compared to those without the condition. The study suggests a correlation between the concentration of estradiol and the development of scoliosis, proposing these hormonal markers as indicators of normal sexual maturation and potential indices for identifying pathologies such as scoliosis (Kulis et al., 2015).

Moreover, genetics also plays a crucial role, and various studies employing cytogenetic analysis, single nucleotide polymorphism tagging, and genome-wide investigations have identified several genes associated with idiopathic scoliosis in humans. One such gene is gamma-1 syntrophin (SNTG1), a component of the dystrophin-associated protein complex that directly interacts with the C terminus of dystrophin, making it a potential candidate involved in idiopathic scoliosis. Another candidate is chromodomain helicase DNA binding protein 7 (CHD7), known for its association with charge syndrome. Additionally, melatonin receptor 1B (MTNR1B), involved in the neurobiological effects of melatonin, has also been implicated in idiopathic scoliosis (Wise et al., 2008).

1.3 Mechanical force and scoliosis

One factor that has received attention as a possible cause of spinal deformity is mechanical forces (pressure and shear stress). The effects of gravitational forces on human spine is ultimately high. Because mechanical loading contributes to the dynamic growth and alignment of the spine, imbalances in the mechanical forces of the spine may be a major factor in the progression of scoliosis. Anatomically, the unique spatial structure of the human spine and the pattern of mechanical forces along the spinal axis allow the spine to rotate and bend easily. When this motion exceeds a threshold, it induces bony curvature (Xie *et al.,* 2022).

The human spine is surrounded by paraspinal muscles crucial for maintaining spinal integrity. Studies have reported that individuals with scoliosis exhibit asymmetrical electromyographic activity in the paraspinal muscles, which could contribute to the progression of scoliosis (Lu et al., 2002). This suggests that asymmetrical mechanical forces may be a causative factor. The theory of the vicious cycle provides a well-established hypothesis on how mechanical forces contribute to scoliosis progression. This cycle begins with a triggering event that leads to the formation of wedged vertebrae, initiating a curvature in the spine. The resulting uneven pressure on the spine can encourage irregular spinal growth, further intensifying vertebral wedging and perpetuating the cycle of scoliosis progression (Figure 1.4) (Stokes et al., 2006). In addition, as the curvature progresses, the vertebral discs become asymmetrically compressed. Eventually, unequal spinal growth occurs. This unequal spinal growth creates a continual

imbalance of mechanical loading that ultimately increases the severity of scoliosis (Hawes & O'brien, 2006).

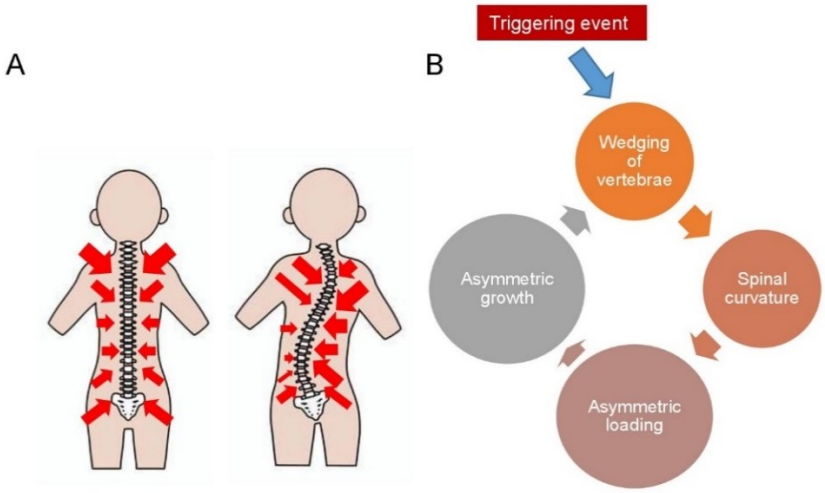

Figure 1.4 Mechanical forces contribute to the progression of Scoliosis. (A) Mechanical forces generated by muscle contraction important to maintain spine integration. Asymmetric forces caused by Abnormal paraspinal muscle contraction cause bone curvature. (B) schematic diagram of vicious cycle theory

1.4 Animal model for studying scoliosis

1.4.1 Mice and chick

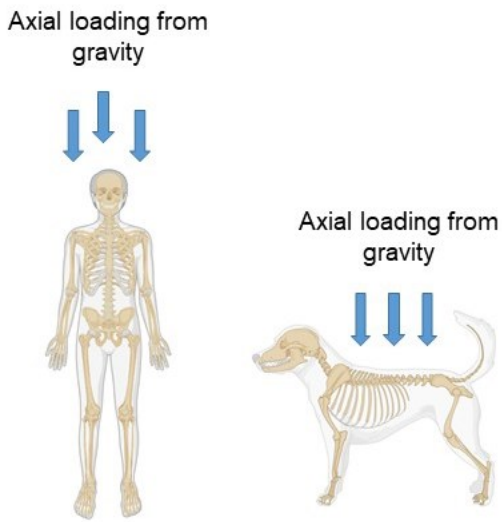

Figure 1.5 Comparison of biomechanical force among bipedal organism and quadruped animal

In humans, it has been suggested that external mechanical forces, such as gravitational forces, may play a role in the onset of scoliosis (Castelein et al., 2005; Xie et al., 2022). Because of

physiologically and anatomically comparable to the human spine, there are many studies using rodent as model of human skeletal disease including scoliosis. However, in the case of scoliosis, the direction of gravity on the spine is different, making common animal models such as mice and rats unsuitable for research. In humans, due to the upright posture, the gravitational load is applied from a direction parallel to the spinal column (Castelein et al., 2005). In contrast, in quadrupedal animals, the direction of the vertebrae and the direction of gravity are perpendicular, so the contribution of gravity to bone growth is quite different (Figure 1.5) (Xie et al., 2022). To address this problem, extreme clinical procedure like forelimbs amputation is always performed to create bipedal mice which mimic the posture of human spine. This procedure requires advance technique and high cost production. whether these models can mimic the actual conditions of scoliosis remains controversial.

Bipedal chicks have been explored as an animal model for studying scoliosis. Researchers have induced scoliosis in chickens through procedures like pinealectomy, indicating that disturbances in the endocrine system and melatonin deficiency may contribute to the development of idiopathic scoliosis (IS). However, it's important to note that the anatomy of the intervertebral joints in chicks differs from that of humans. Chickens have less flexible spinal columns, restricting spinal flexion and extension, which makes them an imperfect model for studying certain aspects of scoliosis (Fagan et al., 2009).

1.4.2 Zebrafish

Interestingly, on the other hand, guppies, zebrafish, and medaka fish are known to spontaneously develop scoliosis. Fish are similar to humans in that during swimming, caudal propulsive forces cause the spine to compress in a direction similar to that of humans which may make fish susceptible to bone kinking (Figure 1.6) (Gorman and Breden, 2009). Moreover, the spine structure between human and zebrafish is comparable. Vertebrae are evenly spaced from the anterior to posterior and display bony arches. Zebrafish precaudal vertebrae are associated with rib segments, as is observed for human thoracic vertebrate. Fish also exhibit a natural anterior kyphosis similar to bipedal organisms.

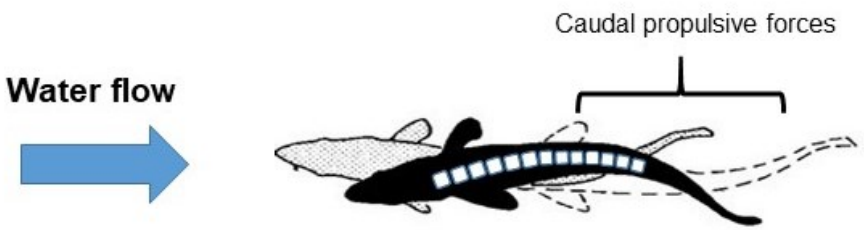

Figure 1.6 Biomechanical force of fish during swimming

Many studies have reported the usefulness of using zebrafish to understand the pathogenesis of scoliosis. For example, irregular cerebrospinal fluid flow caused by abnormal motile cilia can induce idiopathic scoliosis in zebrafish (Grimes et al., 2016;Zhang et al., 2018;Troutwine et al., 2020). Moreover, abnormal muscle fiber has been reported to develop notochord kinks that progress to scoliosis in zebrafish (Whittle et al., 2020).

However, since mechanical loading is believed to contribute to scoliosis progression, it is necessary to establish an animal model that is suitable for this issue. There are several genetic lineages in people presumed to be related to scoliosis, one of which is the mechanoreceptor Piezo channels.

1.5 Piezo channel as a Mechanoreceptor

Mechanotransduction is a crucial process for the survival of all living cells, relying on their ability to sense and convert various mechanical forces, such as touch, hearing, pain, and proprioception, into biological signals. This fundamental capability is essential for controlling cellular processes like migration, proliferation, and differentiation (Marshall and Lumpkin, 2012). At the cellular level, mechanosensitive (MS) ion channels, G protein-coupled receptors (GPCRs), and integrins serve as mechanosensitive receptors. These receptors directly or indirectly interact with force-sensing elements in the cytosol, such as microtubules and actin proteins. Upon sensing mechanical forces, these receptors transmit signals to the nucleus, potentially influencing gene transcription at the downstream level. Among these receptors, mechanosensitive ion channels provide the fastest means of converting mechanical forces into biological signals (Cox et al., 2019).

Like other ion channels, mechanosensitive ion channels create a membrane potential by allowing ion molecules to pass in and out through their pores via passive diffusion, depending on the electrochemical gradient (Martinac and Poole, 2018). While many ion channels in vertebrates are selectively permeable to specific ions, such as potassium channels responding to mechanical stimuli, certain mechanosensitive ion channels have been identified to allow the passage of a combination of cations like sodium (Na+) and calcium (Ca2+) (Murthy et al., 2017). One such ion channel is piezo.

1.5.1 General properties of Piezo channels.

Coste et al. (2010) identified the Piezo genes through gene screening using multiple silencing RNAs in mouse neuroblastoma cells. Piezos represent the largest pore-forming multimeric ion channels consisting of three subunits arranged in a trimeric complex. When viewed from the top, this trimeric complex forms a propeller-like shape, featuring a central pore beneath a cap region (Fig. 1.7). Each subunit comprises over 2500 amino acids, with 30-40 hydrophobic regions, though it remains unclear whether all 38 segments are transmembrane domains. Upon activation, the concentration of sodium and calcium inside the cell increases, leading to signal propagation and initiation of various secondary signaling pathways (Murthy et al., 2017).

Within vertebrates, there exist two types of Piezo genes, sharing approximately 42% sequence homology (Coste et al., 2010). The Piezo1 gene is primarily expressed in non-sensory tissues and is responsible for detecting local changes in fluid pressure. In contrast, the Piezo2 gene is located in neuronal tissues and certain mechanosensory structures (Murthy et al., 2017).

To gain insights into the physiological functions of the Piezo channel, several studies using drug treatment. For instance, Yoda1, the sole known activator of Piezo1 that does not affect Piezo2 activity, has been identified. Yoda1 can be utilized to validate downstream signaling mediated by calcium(Syeda et al., 2015). Both Piezo1 and Piezo2 can be inhibited by GsMTx4, a drug derived from spider venom. GsMTx4 functions by blocking stretch-activated cation channels, inducing changes in membrane curvature around the channel (Bae et al., 2011).

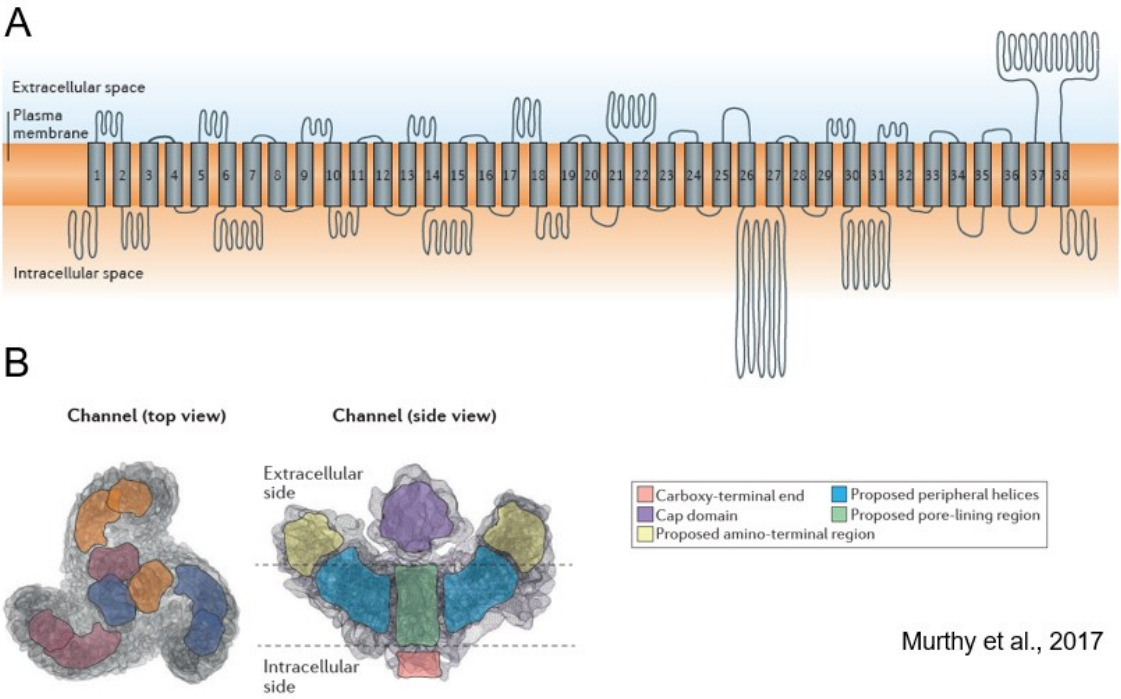

Figure 1.7 Piezo channel. (a) Predicted topology map of PIEZO1 protein depicting 38 putative transmembrane segments (b) shape of piezo channel based on cryo-electron microscopy density map (Murthy et al., 2017).

1.5.2 Activation mechanism

To comprehend the activation of Piezo channels and other types of mechanosensitive ion channels, two hypothesized mechanisms have been proposed. The first model, termed "force-from-lipid," suggests that when force or stimuli are applied, the conformation of the bilipid membrane (lipid-protein interaction) undergoes changes, leading to the opening of the ion channel (Arnadóttir and Chalfie, 2010). This model aligns with mechanically activated ion channels in bacteria and the two-pore domain potassium (K2P) channel family in some vertebrates (Brohawn et al., 2014). The second hypothesis, "force-from-filament," explains that channel opening is driven by cytoskeletal proteins or the extracellular matrix tethered to the ion channel. This mechanism can be observed in Homotetrameric NOMPC (no mechanoreceptor potential C) channels (Arnadóttir and Chalfie, 2010).

Activation of the Piezo channel is thought to be compatible with both models. In one study, the reconstitution of mouse Piezo1 protein in droplet interface bilayers, devoid of other cellular components, demonstrated that rearranging the conformation of the lipid bilayer through mechanical force can open Piezo1. The predicted force required for Piezo1 activation was found to be 3.4 mN/m (Syeda et al., 2016). Conversely, another study supporting the second model revealed that mechanical bending of the apical cell surface using suction or a blunt glass probe led to membrane stretching and activated Piezo1 channel function (Nourse and Pathak, 2017). This strongly suggests that the stretching of the cell membrane aligns with the 'force-from-filaments' principle.

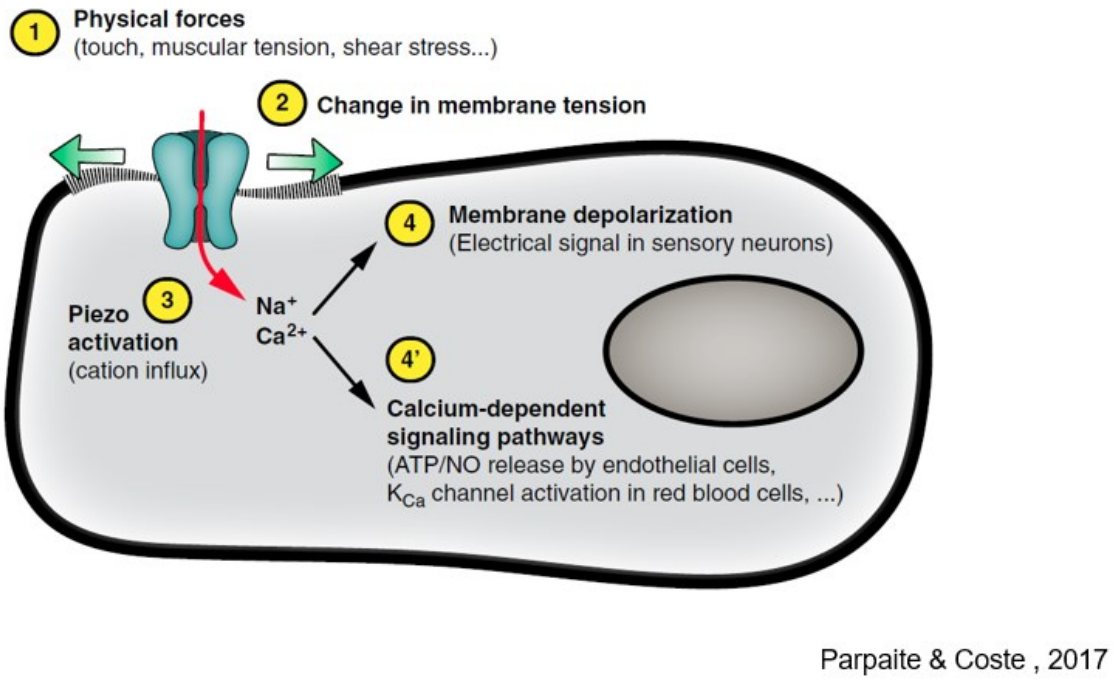

Figure 1.8 Piezo channel activation (Parpaite and Coste, 2017)

Upon activation, the Piezo channel generates currents and depolarizes the membrane potential by permitting the entry of monovalent cations like Na+ and K+, as well as divalent cations such as Ca2+ and Mg2+ into the cell. The opening of the Piezo channel allows calcium ions to enter the cell, initiating intracellular calcium signaling pathways (Fig. 1.8) (Parpaite and Coste, 2017).

1.5.3 Bone, mechanical forces, and Piezo channel

Numerous studies have proposed that mechanical stimuli, such as gravitational force and physical exercise, impact bone formation. For instance, research indicates that mice subjected to microgravity conditions, simulating a space environment, experience considerable bone mass loss. Conversely, exposure to hypergravity significantly increases bone mass in mice (Tominari et al., 2019). Moreover, physical exercise has been shown to enhance bone formation and prevent osteoporosis (Tong et al., 2019). Recognizing the importance of mechanical force, bones' ability to respond to these stimuli is crucial for developing the appropriate bone structure and is essential for the healing process following injury or bone fractures.

Several studies propose that osteocytes, the cells embedded deep within the bone, are responsible for sensing mechanical stimuli. Osteocytes play a role in regulating bone remodeling by releasing biochemical molecules that influence the activity of osteoblasts (bone-promoting cells) and osteoclasts (bone-resorbing cells) (Haelterman and Lim, 2019). A specific study indicates that when exposed to mechanical loading, osteocytes release prostaglandins that impact the function of both osteoblasts and osteoclasts (Raisz, 1999). Furthermore, considering that osteocytes are derived from osteoblasts, it is suggested that osteoblasts may also be sensitive to mechanical loading exposure.

Sun et al. conducted an investigation where they observed that pre-osteoblast cells respond to mechanical force in the presence of Piezo1, utilizing patch clamp techniques coupled with mechanically evoked cationic currents using a glass pipette. They further demonstrated that the knockdown of Piezo1 in pre-osteoblast cells results in reduced gene expression of alkaline phosphatase (Alp), osteocalcin (Bglap), and collagen 1 (Col1a1)—important markers for differentiating osteoblasts. These findings suggest that Piezo1 can mediate the differentiation of osteoblasts in response to mechanical loading stimulation. Subsequently, through conditional knockout experiments in mice, where the Piezo1 channel function was specifically eliminated in osteoblasts and osteocytes, bone formation impairment was observed. The mutant bone displayed a brittle phenotype with low bone mineral density. Osteoblasts lacking Piezo1 exhibited lower mechanically-induced ion currents compared to the control. Notably, when the mutant bones were exposed to mechanical loading treatment (either increased or decreased), the bone mass remained unaffected (Sun et al., 2019).

In contrast, studies have shown that the expression of the piezo2 gene in osteoblasts and osteocytes is low (Li et al., 2019). This observation aligns with research demonstrating that the loss of piezo2 in osteoblast lineage cells does not lead to abnormal skeletal development in mice, suggesting a limited contribution to bone development and homeostasis. Intriguingly, a double conditional knockout of Piezo1 and Piezo2 in mesenchymal cells (bone cell progenitors) resulted in more severe bone defects compared to the single conditional knockout of Piezo1. The more pronounced defects included increased bone fractures, shorter long bones, significantly reduced cortical and trabecular bone mass, and decreased expression of bone marker genes. This implies that Piezo1 is crucial in bone formation, while there appears to be functional redundancy between Piezo1 and Piezo2 in bone-related processes (Zhou et al., 2020).

1.6 Piezo channel and scoliosis

It has been confirmed that *piezo1* genes are highly expressed in mesenchymal stem cells, osteoblasts, chondrocytes, and nucleus pulposus cells of intervertebral disc of the spine (Zhu et al., 2021). This underlines that *piezo1* might contribute to several bone metabolic and degenerative diseases such as osteoporosis, idiopathic scoliosis, or intervertebral disc degeneration. In a recent study, bipedal mice that suffered from scoliosis exhibited asymmetric *Piezo1* expression due to different compression stress of growth plate area. This will induce different degrees of apoptosis of chondrocyte as well as bone growth in growth plate that eventually lead to bone wedging. (Chen et al., 2023). Furthermore, another study demonstrated that patients with osteoporosis had significantly lower *PIEZO1* expression accompanied with low osteoblast marker genes (Sun et al., 2019). In addition, recent clinical report has revealed novel mutations in *PIEZO1* in patients with primary lymphatic dysplasia with symptoms of facial bone hypoplasia, thoracolumbar scoliosis, and short stature (Lee et al., 2021).

On the other hand, *PIEZO2* gene is important in proprioceptive function and is mainly expressed in muscle spindle and the Golgi tendon organ. One study reported that loss of *Piezo2* in the proprioceptive system induces abnormal alignment of spine and misshapen joint in mice (Assaraf et al., 2020). In human, mutation in this gene can lead to several skeletal abnormalities including arthrogryposis, spinal fusion, scoliosis, and hip dysplasia (Haliloglu et al., 2017;Uehara et al., 2020). Therefore, the abovementioned studies demonstrate the importance of Piezo channel in skeletal development.

1.7 Thesis overview

A

Percent identity matrix

	piezo1	piezo2a	piezo2b
Piezo1	100%	47.76%	46.02%
Piezo2a	47.76%	100%	65.60%
piezo2b	46.02%	65.60%	100%

B

Phylogram

C

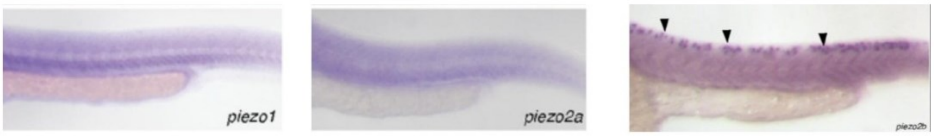

Faucherre et al., 2013

Figure 1.9 piezo genes in Zebrafish. (A) Percent similarity index and (B) Phylogram of piezo1, piezo2a, and piezo2b. Although piezo1 and piezo2a have almost 50% similaties, the expression pattern between both genes is overlapping.

In this study, we proposed that optimal sensing of mechanical force is crucial for the pathogenesis of scoliosis, not just the force itself. To investigate this, we disrupted the ability of zebrafish to sense mechanical force by knocking out *piezo* genes. Zebrafish have three *piezo* genes in their genome (*piezo1*, *piezo2a*, and *piezo2b*). Although piezo1 and piezo2a are not paralog genes, the expression patter is almost similar which broadly expressed throughout the body (Figure 1.9). In addition, piezo2b are only expressed in neuron especially in rohon-beard cell.

Surprisingly, when we deleted both *piezo1* and *piezo2a* simultaneously or introduced an in-frame mutation of *piezo1*, the fish exhibited symptoms similar to bone diseases, including scoliosis and bone degeneration. These findings indicate that zebrafish with deleted *piezo* genes could serve as an animal model for studying scoliosis. Our results provide valuable insights into the role of Piezo channels in bone development and may shed light on potential causes of skeletal disorders.

Chapter 2

2. Material and Method

2.1 Zebrafish Husbandry

All experiments in this study were conducted in accordance with the prescribed guidelines and approved protocols for the handling and use of animals at Osaka University. Tübingen (Tü) strain was used as the wildtype zebrafish and all fish were maintained under standard conditions. Fish were kept under a photoperiod of 14 h light/10 h darkness at 28 ^{O}C in a fish breeding room. Embryos were obtained by crossing mature males and females at 28 ^{O}C. Embryos were collected and incubated in a thermostatic incubator at 28.5 ^{O}C. After hatching, larvae were transferred to the fish breeding room and fed paramecia until they grew to be able to eat artificial diets.

2.2 Generation *piezo1* and *piezo2a* Knockout zebrafish by CRISPR/Cas9 system

For generating zebrafish mutant, CRISPR/Cas9-mediated method was utilized. The sgRNA target site for each gene was designed using crisprscan.org. The sequences of the oligonucleotide for sgRNA are listed in Table 1. To Knock-out *piezo1* and *piezo2a* gene, exon 5 of *piezo1* with target sequence 5' CCTCAGGGTGTGCTGTGGCTCCT 3' and exon 4 of *piezo2a* with target sequence 5' TGGCCACGCTCATCCGCCTCTGG 3' were chosen. For sgRNA transcription, the template DNA was made by polymerase chain reaction using oligonucleotide containing target exon and tracrRNA backbone. Then, about 50 ng synthesized template DNA was *in vitro* transcribed using *in vitro* Transcription T7 Kit (for siRNA Synthesis) (Takara bio), treated with DNase I (Takara Bio), and purified by RNA clean and concentration kit (Zymo Research).

Table 2.1: **Oligo sequences used for CRISPR-Cas9 gRNA generation**

Gene	Primers name	Sequences
piezo1	piezo1 sgRNA exon 5	GCT AAT ACG ACT CAC TAT AGG GAG CCA CAG CAC ACC CTG GTT TTA GAG CT
piezo2a	piezo2a sgRNA Exon 4	GCT AAT ACG ACT CAC TAT AGG GCC ACG CTC ATC CGC CTC GTT TTA GAG CT
piezo1 in-frame mutant (11aa del)	piezo1-sg1F	TAG GAG CGA AAT ATG CAG GCT G
	piezo1-sg1R	AAA CCA GCC TGC ATA TTT GCG T
mstnb	mstnb-sg1-F	TAG GAG CCT TCC ACA GCC ACG G
	mstnb-sg1-R	AAA CCC GTG GCT GTG GAA GGC T

2.3 Generation *piezo1* in-frame mutant zebrafish by CRISPR/Cas9 system

To generate *piezo1* in-frame mutant, an effective single guide RNA (sgRNA) sequence for zebrafish *piezo1* had been reported previously (Gudipaty et al., 2017). This sgRNA targeted the splice acceptor sequence of exon 2 of zebrafish *piezo1* gene. The target sequence is 5'-cagCCTGCATATTTCGCTAC-3' (exonic sequence is shown in uppercase, intronic sequence in lowercase). The 20 nucleotides sequence upstream of PAM were cloned into pDR274 plasmid containing RNA loop structure sequence required for recognition by Cas9 enzyme, and T7 promoter sequence that allowed for *in vitro* synthesis of sgRNA using MEGA Script T7 Kit (Invitrogen #AM1334). Synthesized sgRNA was mixed with Cas9 protein (NEB# M0646T) just before microinjection into zebrafish embryo.

2.4 Microinjection and genotyping

One-cell stage zebrafish embryos were injected with 1-2 nl of injection solution containing 300 ng/µl of Cas9 protein (NEB# M0646T) and 12.5 ng//µl of sgRNA. For genotyping, the DNA was extracted from embryos at 3 dpf or amputated caudal fin at adult stage. These samples then were incubated in DNA extraction buffer supplemented with Proteinase K at 55 ^{O}C for 2 hours and 95 ^{O}C for 5 minutes. The extracted samples were diluted 300 times using distilled water and about 1 µl of diluted sample was used as a template for 20 µl standard PCR amplification. Primers for genotyping are listed in Table 2.

Table 2.2: **Primers used for genotyping**

Gene	Primers	Sequences
piezo1	piezo1 int-4F	TCC TGG GAC GTA ACA AAG CA
	piezo1 int-5R	AGG CCC AGA CTA ACA GCA TT
piezo2a	piezo2a int-4F	TTT GAC AAC AAA ATG ACT CAC TAA TTG
	piezo2a int-5R	CGA TGT ACA AAA AGC CAC CA
piezo1 in-frame mutant (11aa del)	piezo1 int-1F	AAA ATC ACA GCA GGG TGA AT
	piezo1 int-2R	GGC AGA CTA TTG CAA CAT TGA
mstnb	mstnb-ex1F	ACA TCC TTT AGC ACG CCT TG
	mstnb-int1R	CTG CGT AAA GGG TCT CTC CA

2.5 Micro-CT

To analyze bone morphology and phenotypes in detail, utilize micro–computed tomography (micro-CT) is used. Whole-body fish was fixed in 4% PFA overnight. Fixed samples were observed by micro–CT-scanner SkyScan 1,172 (SkyScan NV, Aartselaar, Belgium) following the manufacturer's instructions. The X-ray source ranged from 50 kV, and the datasets were acquired at a resolution of 5 µm/pixel for abdominal or caudal part and 12 µm/pixel for whole body, depending on the size of each vertebral body. Samples were scanned in air dry condition. Neural arches and hemal arches were not included in bone analysis. After applying a fixed threshold for all samples, 3D evaluation is conducted using CTVox and CTAn. Orthoslice images were obtained using Dataviewer (Bruker, Kontich, Belgium).

2.6 Alizarin Red S staining

For live imaging, fish at larvae (8 dpf), juvenile (20 dpf), and young adult (35 dpf) were incubated in 0.005% alizarin red S (Sigma) overnight and washed three times with tank water. Before observation, samples were anesthetized using *Ethyl 3-aminobenzoate methanesulfonate*. Imaging was performed on a BZ-X710 Keyence fluorescence microscope.

2.7 Histology and Alkaline Phosphatase staining

Since alkaline phosphatase is an enzymatic reaction, fixation and long incubation time in chemical solution will affect the result. To address this problem, we perform Kawamoto's film method using fresh and unfixed samples (Kawamoto, 2003). Briefly, fish at 3 months were anesthetized and then cut into three pieces. The cut samples were embedded into embedding medium before being soaked in cooled isopentane with liquid nitrogen. Using cryofilm tape, samples were sectioned at 20 μm thickness. Sections were fixed with 4% PFA for 5 minutes then washed three times using PBS. Takara TRACP & ALP double-stain Kit was used for the detection of alkaline phosphatase according to manufacture. Staining was performed at room temperature for 30 minutes.

2.8 RNA extraction and cDNA synthesis

To perform relative mRNA expression analysis, total RNA was extracted from vertebral bone using RNeasy Lipid tissue mini kit (QIAGEN) according to the manufacturer′s protocol. Subsequently, RNA concentration was measured using Q5000 micro-volume spectrophotometer (TOMY). About 500 ng of extracted RNA was used for cDNA synthesized using ReverTra Ace qPCR RT kit following the manufacturer′s protocol. The cDNA was stored at -20 ^{O}C until use.

2.9 Cell-attached patch clamp mode

To confirm whether the 11 amino acid deletion affects Piezo1 channel function, we performed patch-clamp experiment using cell-attached mode. The cDNAs of zebrafish wildtype-*piezo1* and 11-amino acids deletion mutant were cloned into pIRES2-GFP vector, respectively. The constructed plasmids then were purified using nucleospin plasmid-transfection grade (TAKARA) and transfected into piezo1-deficient N2A cells (Sugisawa et al., 2020). About 48 to 72 hours after transfection, the channel activities were recorded.

Briefly, the recordings were conducted at room temperature with a mean pipette resistance of 4.0 to 6.0 MΩ. In this recording, the pipette solution contained 140 mM NaCl, 5 mM KCl, 2 mM $MgCl_2$, 2 mM $CaCl_2$, 10 mM hepes (pH 7.4 adjusted with NaOH), and 10 mM glucose same with bath solution. Following giga-seal formation, the holding potential was clamped to -80 mV and the channel was stimulated by applying a negative pressure of -40mmHg.

2.10 qPCR

The primers for this experiment are listed in supplementary table S3. To perform qPCR analysis, SYBR Green PCR Master Mix (Applied Biosystem) was used and carried out in the Applied

Biosystems™ StepOne™ Real-Time PCR System. The amplification conditions were 95 °C for 10 min, 40 cycles at 95 °C for 15 s, and 60 °C for 1 min. All reactions were performed in triplicate. Relative mRNA expressions were normalized to *beta-actin* (*actb1*) gene. Primer sets for qPCR were listed in Table 3.

Table 2.3: Primers used for qPCR

Gene	Primers	Sequences
piezo1	piezo1 QPF	GAG AGG ATG CGG CTT CTC AA
	piezo1 QPR	CCA CAT GGT GAA TCC GTC CA
piezo2a	piezo2a QPF	CCG GAT AAC TAC ACC GAG GC
	piezo2a QPR	CCA GCA GGG GAC TGA ACT TT
osterix	osterix QPF	GAC CCT CAC TGG ACT GCT TC
	osterix QPR	CGA ATT TGT TGC AGG TCG CA
bglap	bglap QPF	CAG TCC TGA TCT TCT GCT GCC
	bglap QPR	CAC GCT TCA CAA ACA CAC CTT CAT

2.11 Rescue experiment with introducing functional *piezo1*

Zebrafish *piezo1* coding sequence (CDS) was amplified by PCR and then cloned into the pTol2 plasmid with *osterix* promoter (Kawakami et al., 2000;Renn and Winkler, 2009). Sequences of the primers used to amplify *piezo1* CDS are piezo1-F1_Sal1; 5-TTTTGGCAAAGAATTGTCGACCACCATGGAGCTTCAGGTGGTA-3' and piezo1-R1_Not1; 5'-CGTTAGGGGGGGGGGGCGGCCGCTCAGTTGTGATTCTTCTCTC-3'. In addition, since Piezo1 protein has many hydrophobic domains that cause toxicity in *E. coli*, intron 10 and intron 42 were inserted in CDS. Purified plasmid was mixed with *in vitro* synthesized Tol2 Transposase mRNA (10 ng/μL each), and the mixture was injected into fertilized eggs (1 nL/egg) at the single-cell stage.

2.12 Statistical analysis

All data are presented as mean ± SD. Statistical analysis was performed by two-tailed Student's t-test for the two groups and by one-way analysis of variance (ANOVA) test and Tukey's post-test for the three groups. Differences were considered statistically significant at $P < 0.05$.

Chapter 3

3. Results

3.1 Generation of piezo null mutant

Zebrafish have three different *piezo* genes: *piezo1* (XM_691263), *piezo2a* (XM_021470255), and *piezo2b* (XM_021468270). In whole-mount *in situ* hybridization using 48hpf larval zebrafish, both expressions of *piezo1* and *piezo2a* were detected in many tissues, including bone, while *piezo2b* expression was limited to cells of the nervous system (Faucherre et al., 2013). This suggests that zebrafish *piezo1* and *piezo2a* may have redundant functions.

To generate *piezo* activity-deficient zebrafish, the CRISPR/Cas9 method was used (Ran et al., 2013). A guide RNA targeting the internal sequence of exon 5 of *piezo1* gene or exon 4 of *piezo2a* gene was synthesized and co-injected with Cas9 protein into one-cell stage wildtype embryos. Following the screening of several founders that transmitted to the F1 progeny, I established two independent stable lines of each mutant gene. I verified the sequence of each mutant allele and confirmed that each mutant gene generated a premature termination codon (PTC) as a result of an altered mRNA reading frame (Figure 3.1A-D).

I assessed the relative mRNA levels of *piezo1* and *piezo2a* in each homozygous mutant, but observed no significant changes in expression. This suggests that the Non-mediated mRNA decay (NMD) pathway may not have occurred (Figure 3.1E-F).

3.2 Phenotypes of the zebrafish with double mutations of *piezo1* and *piezo2a*

As I expected from the similarity of expression pattern, the single mutants of *piezo1*$^{-/-}$ and *piezo2a*$^{-/-}$ were viable and fertile. Neither mutant showed morphological abnormalities in the larval and juvenile stages (Figure 3.2).

Next, to obtain large numbers of fish with double mutations, fish sharing the *piezo1*$^{-/+}$*; piezo2a*$^{-/-}$ genotype were crossed. In this case, 2-30% of the individuals died around 10 days after fertilization. When the gene was examined, fish with the double homozygous mutation survived to day 8, but all died by day 11 (Figure 3.3A). This indicates that the double mutant fish is lethal in the juvenile stage.

The surviving fish on day 8 showed a shortening of body length (Figure 3.3B) and curvature of the body axis (Figure 3.3C, 3.3D). In addition, the swim bladder was not fully inflated (90%) (Figure 3.3D arrowhead). Alizarin red S staining revealed that all double homozygous mutants showed inadequate bone formation such as small vertebral segment, hemivertebral and vertebral bone missing compared to their siblings (Figure 3.3E-3.3H).

From these data, it is shown that Piezo channels are essential for bone formation and mineral deposition during early development. However, because of the lethality in the young stage, it is not suitable for pathological model of scoliosis.

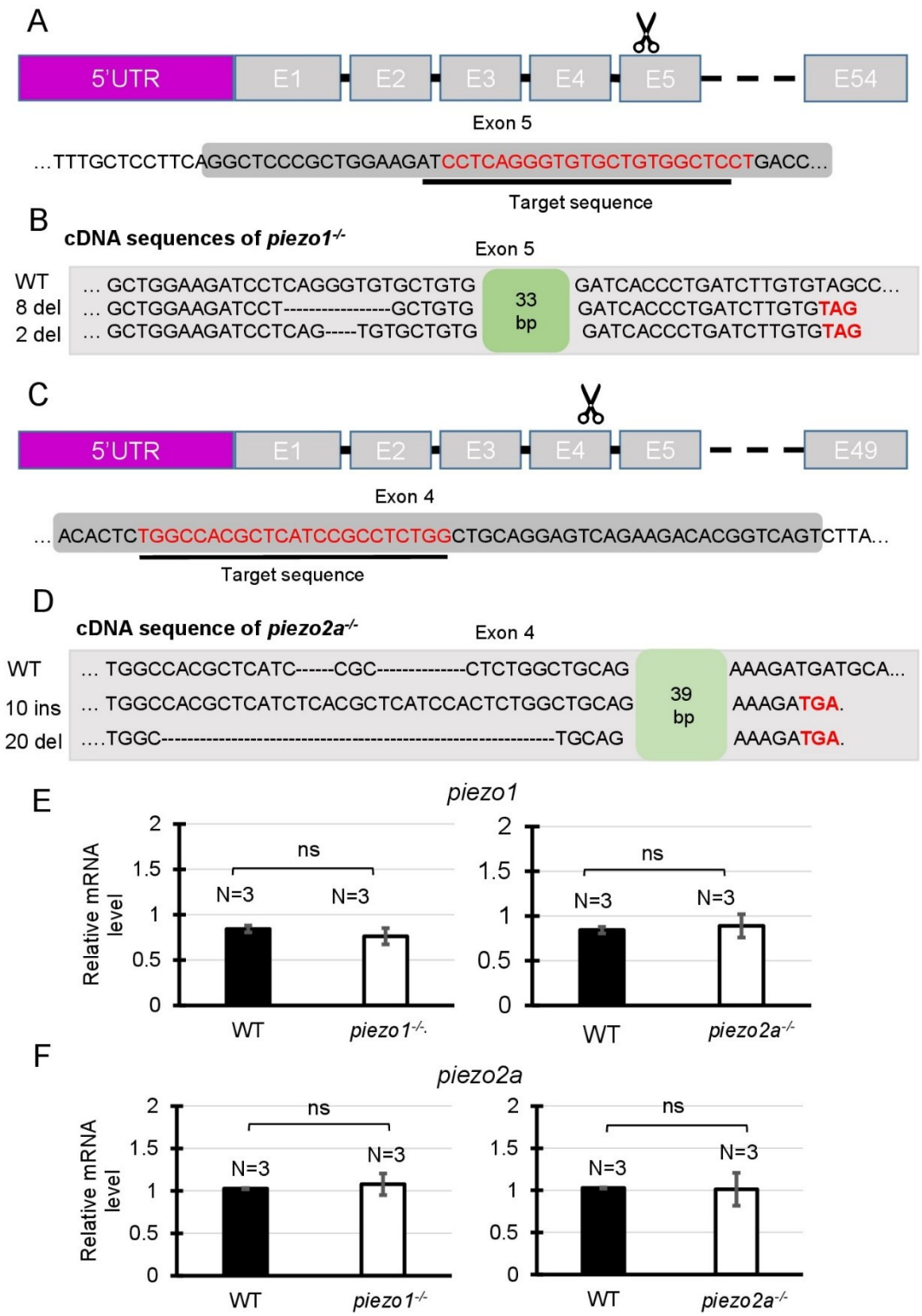

Figure 3.1 Generation of *piezo1*$^{-/-}$ and *piezo2a*$^{-/-}$**.** (A)(C) Schematic diagram of CRISPR/Cas9 targeting of *piezo1* and *piezo2a* genes by guide RNAs targeting the N-terminal regions of *piezo1* exon 5 and *piezo2a* exon 4, respectively. (B)(D) Sequence confirmation of *piezo1*$^{-/-}$ alleles and *piezo2a*$^{-/-}$ alleles showing premature terminator codon. Relative mRNA level of (E) *piezo1* and (F) *piezo2a* in *piezo1*$^{-/-}$ and *piezo2a*$^{-/-}$ mutant fish. No significant changes in the expression of the corresponding genes suggest that transcriptional adaptation and Non-mediated mRNA decay (NMD pathway are not required for genetic compensation in each piezo mutant.

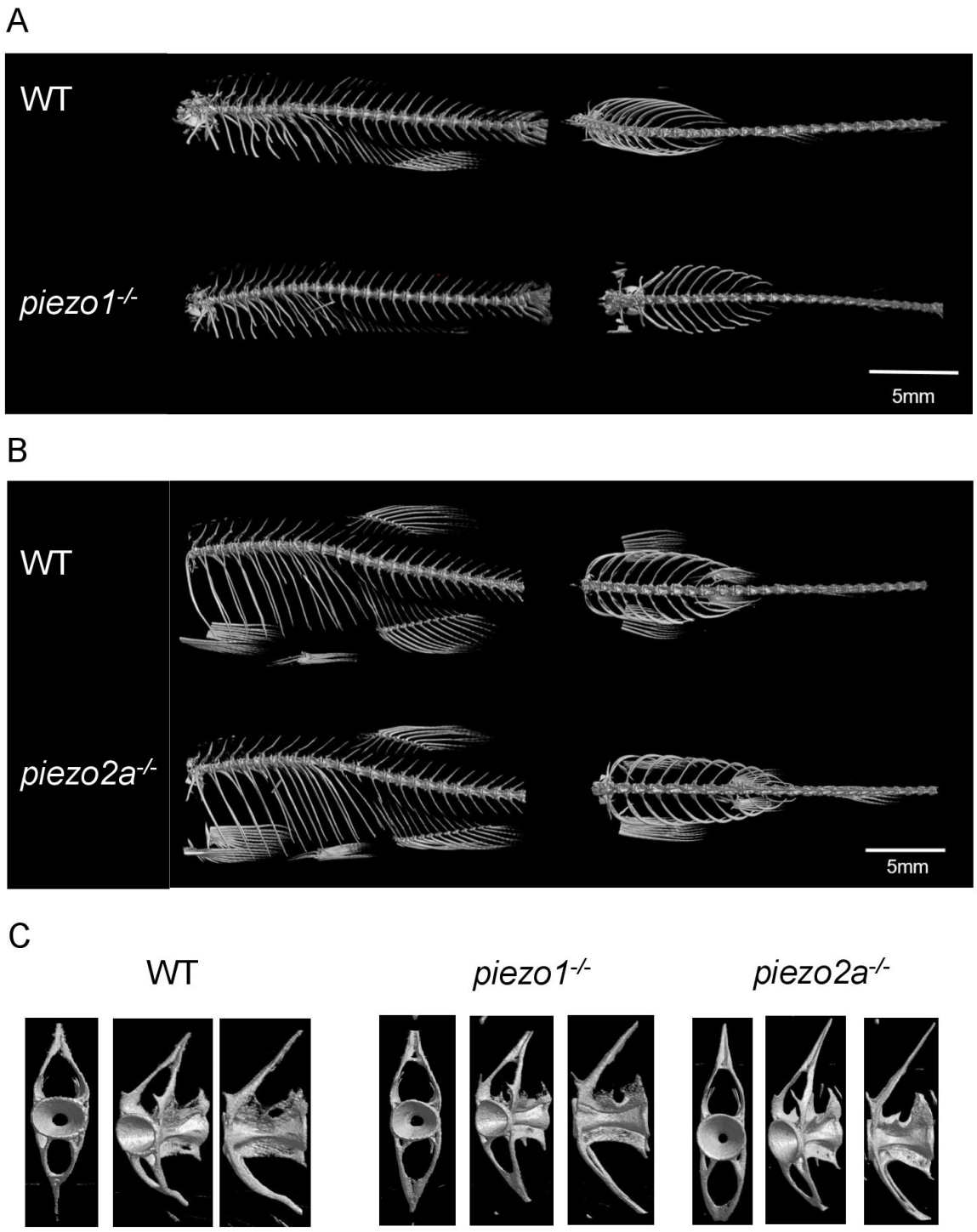

Figure 3.2 C Comparison of 3D reconstruction of micro-CT images of whole body of (A) *piezo1*$^{-/-}$ (N=6) and (B) *piezo2a*$^{-/-}$(N=4). as well as (C) bone segment at 4 mpf. Notably, there were no morphological abnormalities in each null mutant.

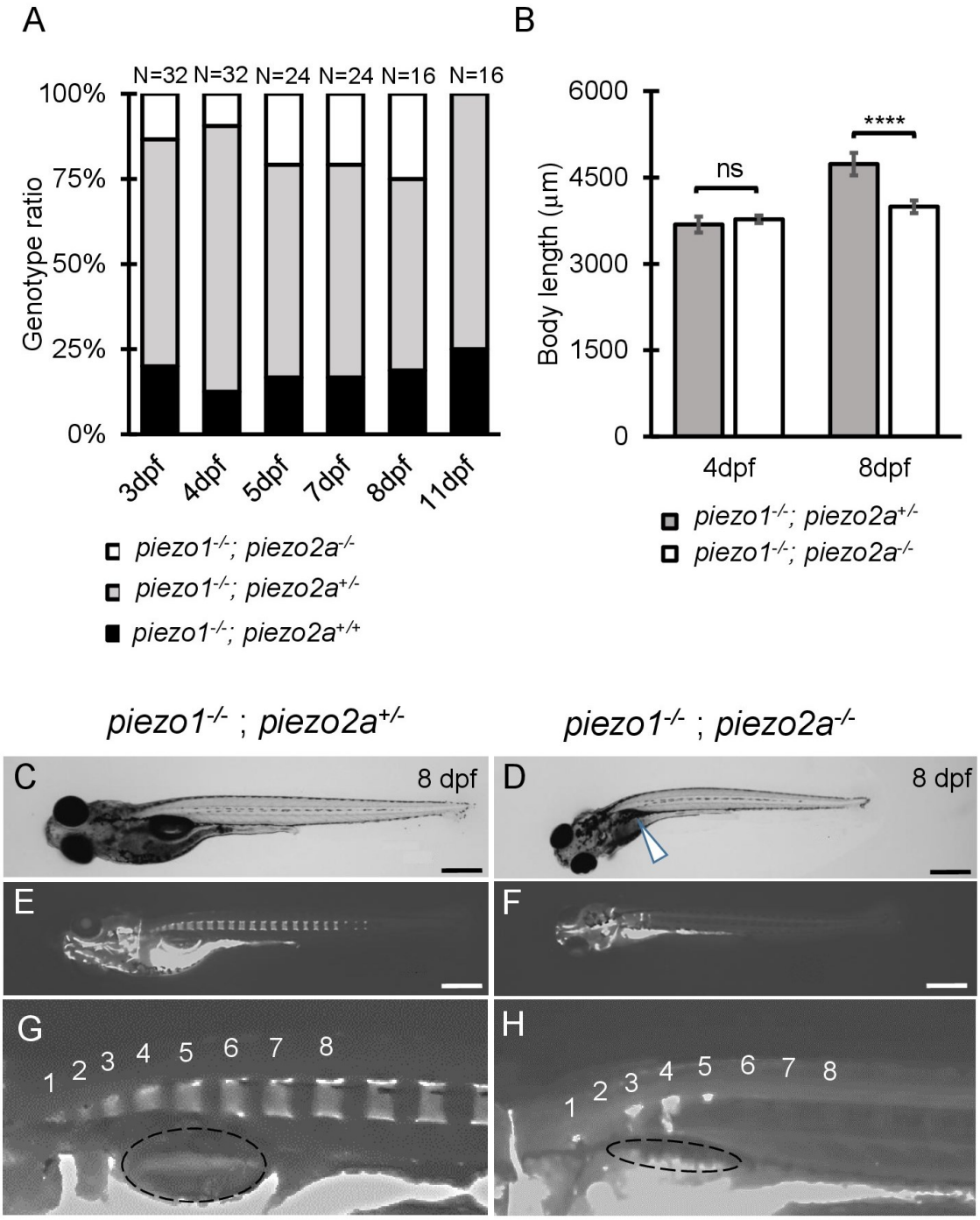

Figure 3.3 *piezo1* and *piezo2a* are essential for bone formation and mineral deposition in early stage of development. (A)(B) Gross phenotypes and (C)(D) mineralization patterns of sibling and *piezo1*$^{-/-}$*; piezo2a*$^{-/-}$ mutant at 8 days after fertilization (dpf). White arrow indicates uninflated swim bladder. Scale = 500 µm. (E)(F) Magnified images of the anterior body of sibling and double mutant. Numbers 1 to 8 indicate the position of each vertebral bone. The dashed circle indicates swim bladder. Notably, the swim bladder in double mutant was small and uninflated. (A) Genotype ratio between double knock out and sibling in several time points. (B) Graph depicting total body length at 4dpf and 8dpf (N=8 for each group). Values are presented as mean ± SD and analyzed using student t-test. **** $P < 0.0001$. ns indicates not significant.

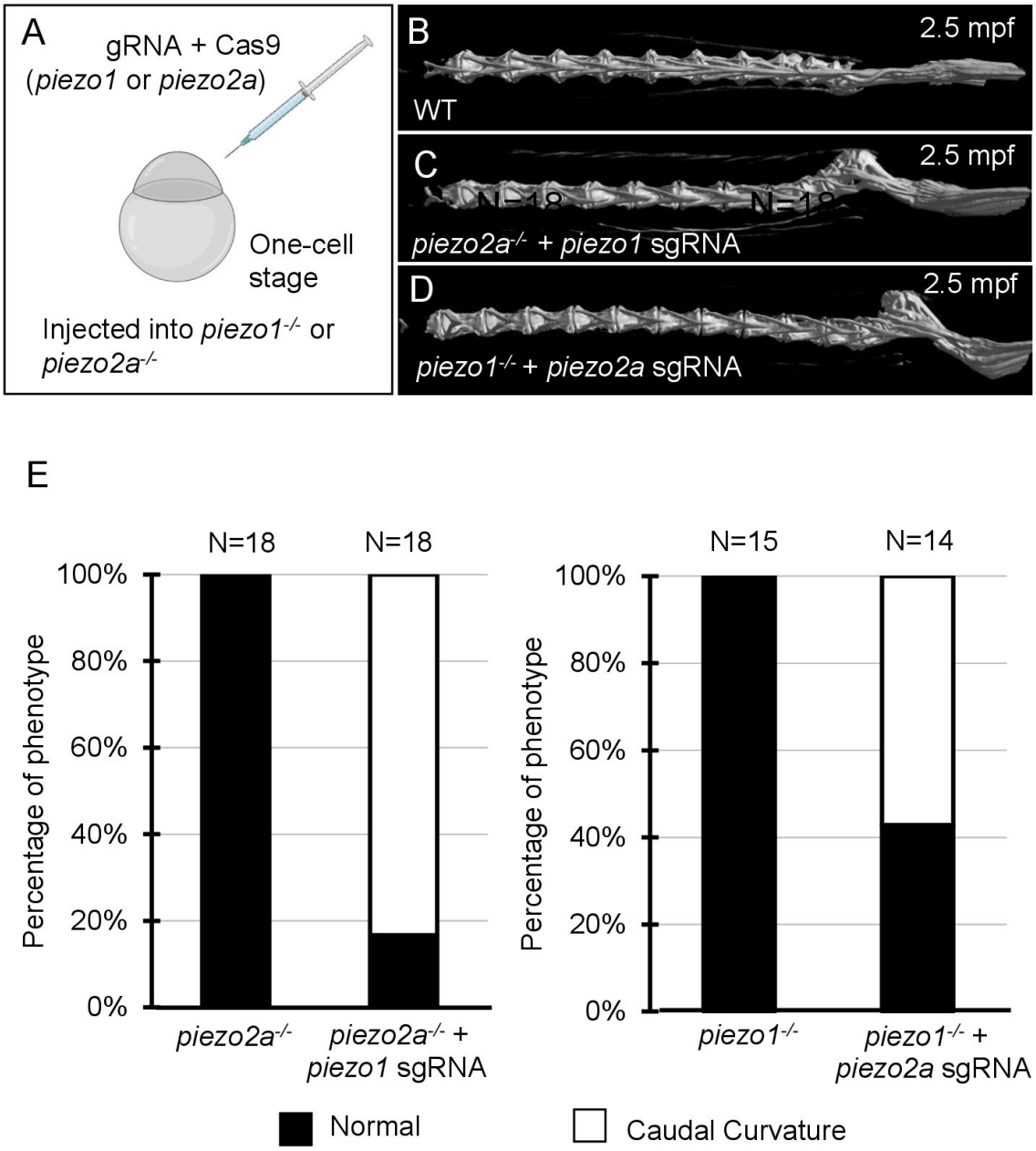

Figure 3.4 Phenotype of piezo mosaic mutant. (A) Schematic diagram of generating piezo transient KO mutant (CRISPRant). Comparison of 3D reconstruction of micro-CT images of vertebral bone at caudal part from (B) wildtype, (C) *piezo1* sgRNA injected to *piezo2a*$^{-/-}$, and (D) *piezo2a* sgRNA injected to *piezo1*$^{-/-}$ at 2.5 months after fertilization. (E) Percentages of abnormal phenotype in mosaic mutant fish.

3.3 Mosaic mutant displays bone curvature

If the cause of death is an abnormality that occurs in an organ other than the spine, CRISPRants (F0 mutants), in which loss of function of the target gene occurs in a mosaic fashion, may avoid the lethality that occurs early in development and allow us to study effects during later developmental stages (She et al., 2019;Buglo et al., 2020). To test this possibility, Iinjected sgRNAs targeting *piezo1* or *piezo2a* into one-cell stage embryos in a *piezo2a* null mutant or *piezo1* null mutant background (Figure 3.4A).

As a result, no abnormal phenotypes were observed in either mutant background at the larval to juvenile stage. However, by 17 days post-fertilization (dpf), a small kink of the spine near the tail of the body occurred. This curvature was even more severe in adulthood in more than 80% of *piezo2a*$^{-/-}$ injected with *piezo1* sgRNA and about 50% of *piezo1*$^{-/-}$ injected with *piezo2a* sgRNA, with the abnormal vertebrae located near the distal end of the tail and near the hypural complex (Figure 3.4B-E)

In this mosaic mutants, the irregular bone morphology shares some similarities with scoliosis, particularly in its occurrence during the process of growth. This fact suggests that artificial mutations in the *piezo* genes may be able to create a pathological model of scoliosis, but in order to create a usable model, lethality must be avoided by simpler methods.

3.4 Generation of *piezo1* in-frame mutant

Next, I analyzed in-frame mutation of the *piezo1* gene. In the process of creating a deletion mutation in the *piezo1* gene, an in-frame mutation was obtained when a guide RNA targeting the splice acceptor sequence in exon 2 was used. In this allele, the removal of the splice acceptor site "AG" resulted in a deletion of 11 amino acids, without the insertion of a premature stop codon (Figure 3.5A,3.5B). The mutant was designated as *piezo1*$^{11aa\ del/11aa\ del}$ and the resulting protein was named 11aa del-Piezo1. The 11 amino acid deletion region is conserved among vertebrates (Figure 3.5.C) and likely plays an important role in Piezo1 channel function.

First, I measured mRNA levels of 11aa del-Piezo1 using qPCR to determine whether *piezo1* gene in *piezo1*$^{11aa\ del/11aa\ del}$ is transcribed normally. The results showed that the mRNA level of *piezo1* in *piezo1*$^{11aa\ del/11aa\ del}$ mutant was reduced by almost half compared to the wildtype (Figure 3.5D), while there was not a significant difference in *piezo2a* mRNA level (Figure 3.5E).

Next, I assessed the channel activity of 11aa del-Piezo1 using a cell-attached patch clamp assay. The zebrafish *piezo1* genes were obtained from both the wildtype and mutant forms, inserted into an expression vector, and transfected into *piezo1*-deficient N2A cells. After about 48 hours of incubation, channel activity was recorded. It was found that in wildtype Piezo1, an inward current flowed when negative pressure was applied with a pipette, whereas only a very weak current flow was observed in the 11aa del-Piezo1 (Figure 3.5E, 3.5F). These results indicated that the deletion of 11 amino acids in the N-terminal domain of Piezo1 caused a functional defect in the Piezo1 channel. In the following experiments, I examined the effects of this on spine formation in detail.

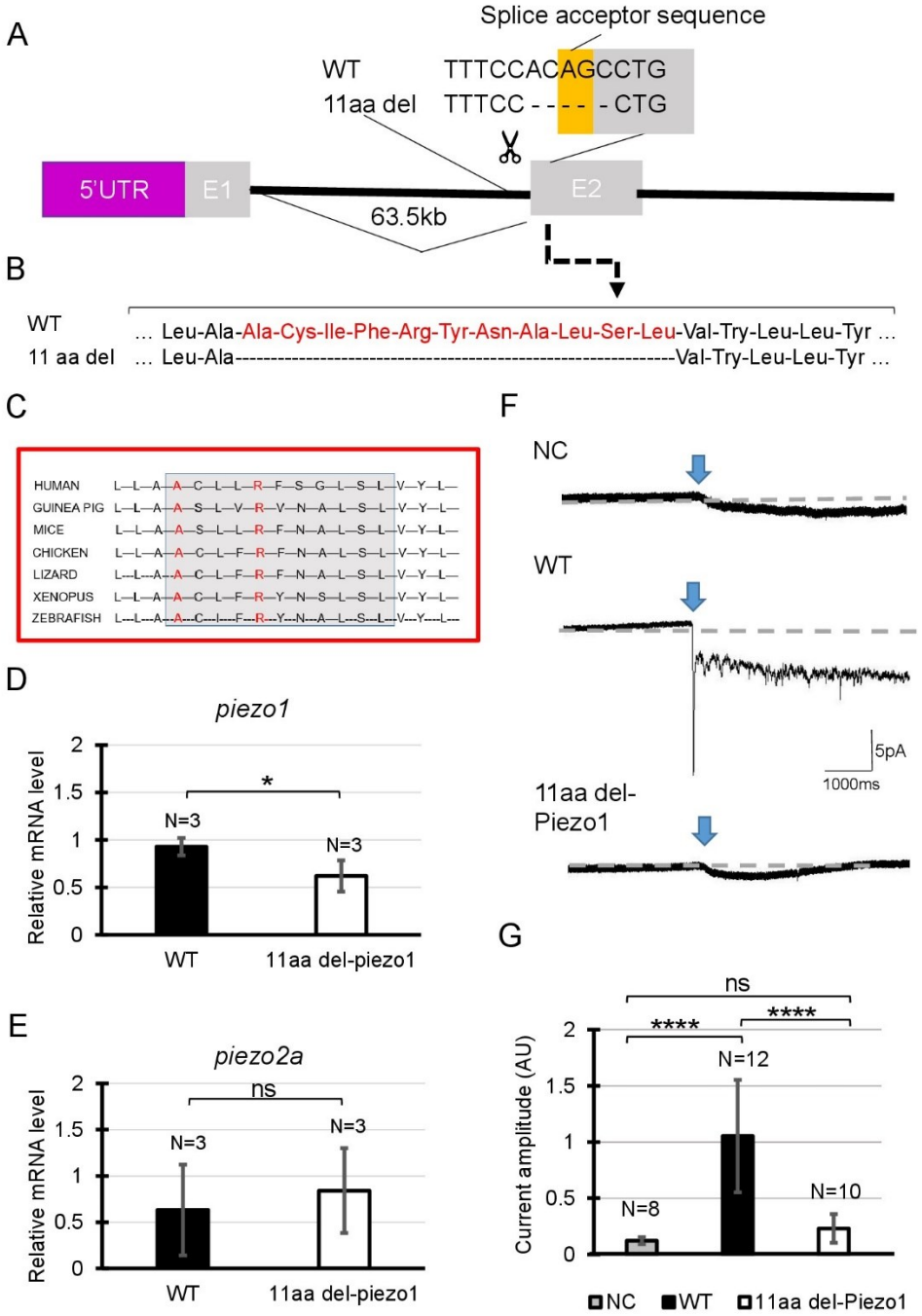

Figure 3.5. Generating *piezo1* in-frame mutant. (A) Schematic illustration of CRISPR target in *piezo1* gene with a guide RNA targeting splice acceptor site of exon2. Through this guideRNA, the splice acceptor site was eliminated, generating cryptic acceptor site which deleted several bases of internal exon 2. (B) Confirmation of amino acid sequence. (C) 11 amino acid deletion region in Piezo1 is highly conserved among vertebrates. Quantification of relative mRNA level of (D) *piezo1* and (E) *piezo2a* in *piezo1*$^{11aa\ del/11aa\ del}$. Values are presented as mean ± SD and analyzed using student t-test. $^{**}P < 0.01$. (F) Representative traces of negative pressure-induced inward currents recorded at -80 mV in negative control (NC), zebrafish Piezo1 Wildtype (WT), and zebrafish 11aa del-Piezo1. Blue arrows indicate the time when negative pressure was applied. Grey dashed lines indicate baseline of the current. (G) Measurement of current amplitude, measured in arbitrary units (AU). Values are presented as mean ±SD and analyzed using one-way ANOVA followed by Tukey's test. $^{****}P < 0.0001$. ns indicates not significant.

3.5 *piezo1* in-frame mutant (*piezo1*$^{11aa\ del/11aa\ del}$) develops juvenile-onset scoliosis

At 4 dpf, there were no critical differences between wildtype and *piezo1*$^{11aa\ del/11aa\ del}$. However, at later stages, during the larval and early juvenile period, the body length of the mutant fish became relatively shorter than that of wildtype, suggesting the late-onset abnormality in the vertebrae (Figure 3.6B).

Alizarin red staining to track vertebral formation at 8 dpf, 20 dpf, and 35 dpf showed that the spines gradually curved as the fish grew, and heterotopic bone formation was occurring in the intervertebral space. Unlike double mutant fish, however, there was no significant variation in the number or spacing of vertebrae or in the morphology of individual vertebrae (Figure 3.6A).

In adults, the curvature of the spine was even more severe, and it appears to be folded in particularly severe areas. This curvature occurs both laterally and vertically (Figure 3.8A). In general, these symptoms resemble human scoliosis (Cheng et al., 2015). To determine the severity of scoliosis, cobb angle was used to measure the degree of spinal curvature. By drawing the parallel lines of the upper border of upper vertebrae and the lower border of lowest vertebrae of the structural curve, then erecting perpendiculars from these line to cross each other, the angle between these perpendicular being the cobb angle or angle of curvature (Bearce et al., 2022). Although sexual dimorphism is one of idiopathic scoliosis features in human, which has also reported in several zebrafish scoliosis mutant model (Hayes et al., 2014;Marie-Hardy et al., 2021), there was no gender bias in *piezo1*$^{11aa\ del/11aa\ del}$ mutant fish. Both sexes developed similar severity of curve penetrance (Figure 3.6E).

3.6 Detailed observation of vertebra shape by micro-CT

Next, micro-CT measurements were taken to examine the shape of the individual vertebrae and surrounding bone (Figure 3.7). As shown in Figure 3.6A, the vertebrae were generally curved, but there were no significant changes in the shape of the neural or haemal arches. To assess the deformity of individual vertebrae causing the curvature, the size of individual vertebrae was measured and expressed as the ratio of anterior/posterior height (H1/H2) and dorsal/ventral length (L1/L2) (Bearce et al., 2022). Figure 3.7A shows data for the 8th to 13th vertebrae of 5 individual fish. In the wildtype, both ratios were approximately 1, with very little variation among individuals or by vertebral position (Figure 3.7C). In the mutant, however, there was variation for each vertebra, and the variation in length ratio (L1/L2) was considerably greater than the variation in height ratio (H1/H2) (Figure 3.7D). This fact suggests that the curvature of the spinal column has caused more longitudinal compression, which is also characteristic of scoliosis in humans (Shea et al., 2004;Schlager et al., 2018).

I also assessed Tissue Mineral Density (TMD) using CT data to evaluate calcium deposition in bones. In general, wildtype fish exhibited high TMD (Figure 3.7E). In the case of *piezo1*$^{11aa\ del/11aa\ del}$, the curved bones exhibited elevated TMD, likely attributable to increased mechanical stress from bone compression (Bagwell et al., 2020). To mitigate measurement bias arising from bone irregularities, I specifically measured TMD in the non-curved bones, particularly focusing on the central portion of the hourglass-shaped bone. I found that *piezo1*$^{11aa\ del/11aa\ del}$ at 3 months of age had predominantly lower TMD values than the wildtype (Figure 3.7E, 3.7F). This is consistent with various reports when they assessed the bone mineral density in scoliotic patients (Sarioglu et al., 2019;Li et al., 2020;Almomen et al., 2021).

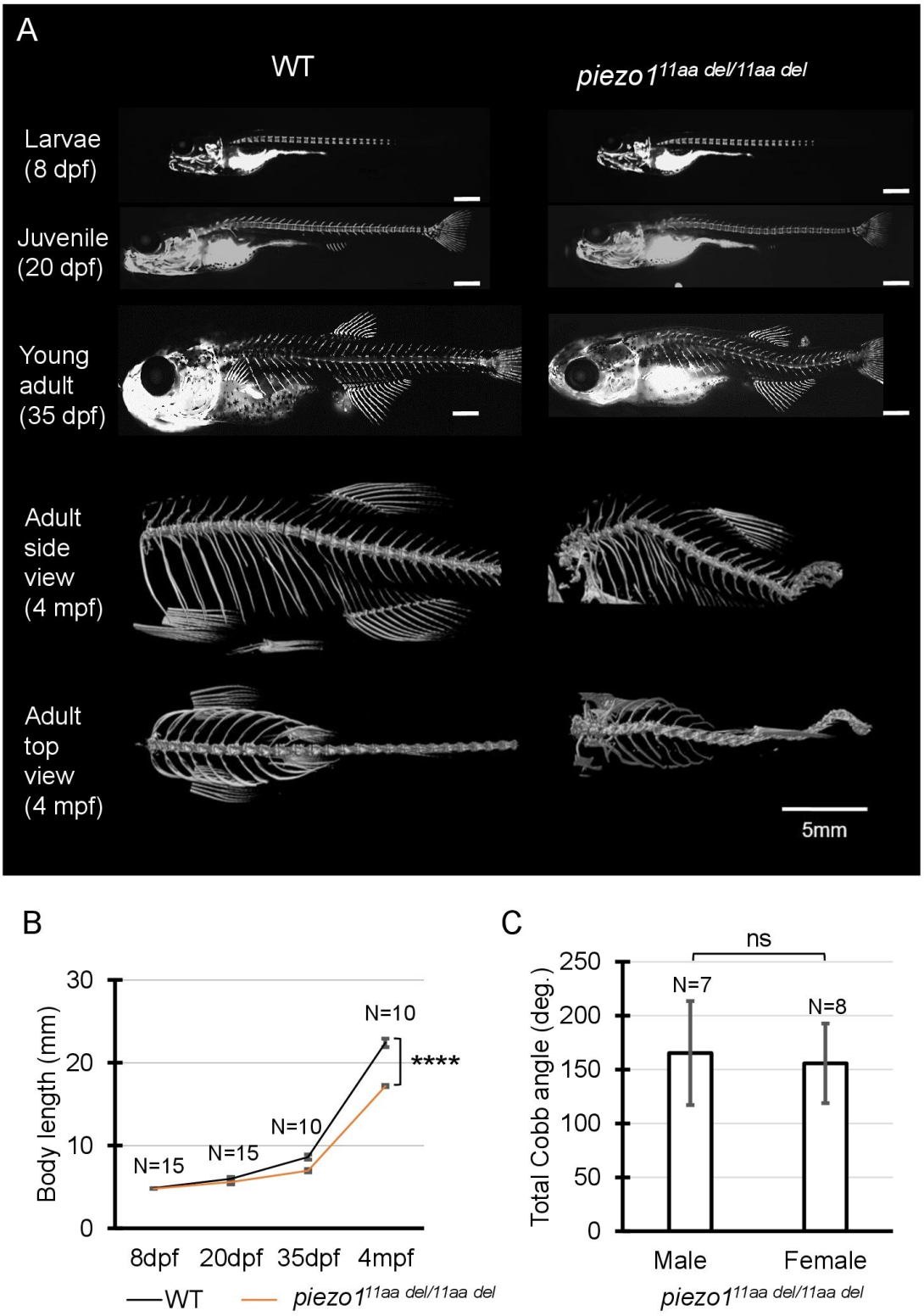

Figure 3.6 Phenotype of *piezo1* in-frame mutant (*piezo1*$^{11aa\ del/11aa\ del}$). (A) Time course observation of mineralized bone using alizarin red S staining between wildtype and *piezo1*$^{11aa\ del/11aa\ del}$ mutant from larvae (8 dpf) to young adult (35 dpf) (Used scale 500 µm) and 3D rendering of micro-CT images of wildtype and *piezo1*$^{11aa\ del/11aa\ del}$ mutant at 4 months. (B) Graph depicting body length. (C) Average of total Cobb angle. Cobb angles were measured according to previous study (Bearce et al., 2022). Values are presented as mean ± SD and analyzed using student t-test. **** $P < 0.0001$. ns means non-significant.

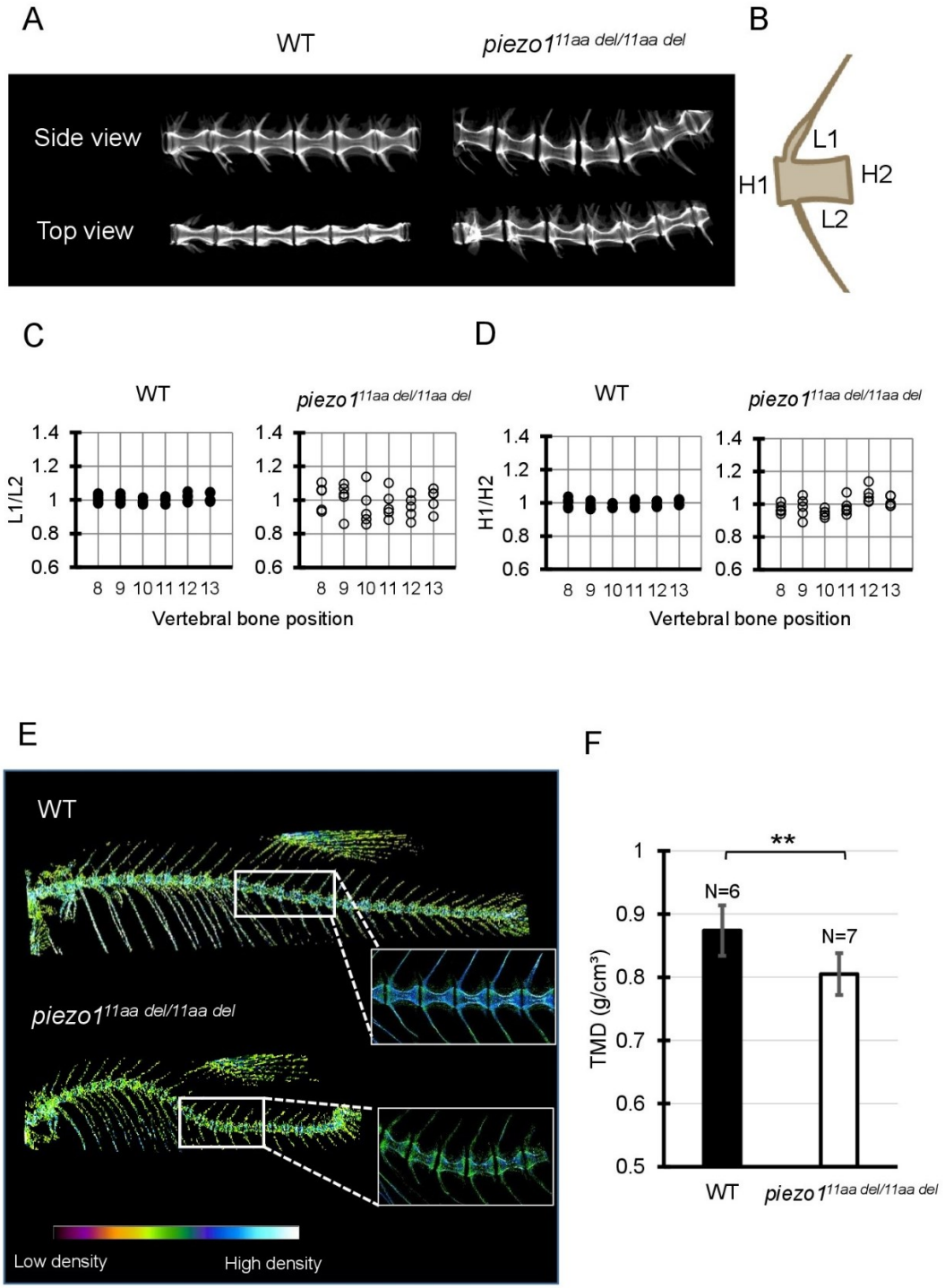

Figure 3.7. Detailed analysis of vertebra shape. (A) Comparison of 3D reconstruction of micro-CT images of vertebral bone between wildtype and *piezo1*$^{11aa\ del/11aa\ del}$ at the abdominal part from side and top view. (B) Schematic diagram and quantification of the (C) length ratio (L1/L2) and (D) height ratio (H1/H2) of single vertebrae measurement. About 6 vertebrae from wildtype (N=5) and mutant (N=5) were assessed. Length aspect ratio and height aspect ratio were significantly more variable in mutant ($P < 0.0001$, analyzed using F-test two samples for variances). (E) The micro-CT reconstructions of 3 months zebrafish from both the wildtype and *piezo1*$^{11aa\ del/11aa\ del}$ mutant specimens were performed. The reconstructions were color-enhanced to represent bone density value. To minimize measurement error, trunk or abdominal part was chosen to measure TMD value due to low bone kinks, indicated as white boxes. (F) Measurement of TMD. Values are presented as mean ± SD and analyzed using student t-test. ** $P < 0.01$.

3.7 Abnormal osteoblast function

Due to the decreased TMD value observed in the mutated bones, I opted to examine the bone metabolism profile. In individuals with osteoporosis, diminished bone density is consistently linked to reduced osteoblast activity or heightened osteoclast activity (Guido et al., 2009). Since previous study has verified the *piezo1* gene expression is higher in osteoblast than osteoclast, I mainly analyzed osteoblast activity using alkaline phosphatase staining (Sun et al., 2019).

Alkaline phosphatase (ALP) is not exclusively produced from bone, but also from liver, kidney, small intestine, and so on. To avoid false observation, fixed region of interest (ROI) was put around growth plate region indicating bone alkaline phosphatase. As shown in figures 3.8A and 3.8B, wildtype fish displayed larger alkaline phosphatase positive area than *piezo1*$^{11aa\ del/11aa\ del}$. Low levels of alkaline phosphatase in scoliotic mutant fish indicate reduced bone formation, as ALP is produced as a byproduct of osteoblast activity.

Furthermore, I generated transgenic fish expressing green fluorescence protein (GFP) in *Osterix* promoter, an osteoblast-specific promoter (Iwasaki et al., 2018). Since GFP-positive osteoblasts are observable in transgenic (*osx-GFP*) larvae, the progression of osteoblast differentiation and the formation of bone can be directly tracked.

The stable transgenic fish (*osx-GFP*) were crossed twice with *piezo1*$^{11aa\ del/+}$ to generate wildtype;(*osx-GFP*) and *piezo1*$^{11aa\ del/11aa\ del}$; (*osx-GFP*) siblings. As expected, *piezo1*$^{11aa\ del/11aa\ del}$ mutant fish exhibited lower GFP signal than wildtype siblings (Figure 3.8C,3.8D). This suggests that not only osteoblast activity is reduced but osteoblast differentiation is also affected in this scoliotic mutant fish.

To further confirm these results, I measured two osteoblast marker genes, *osterix* and *bglap/osteocalcin* by quantitative PCR analysis. As shown in figures 3.8E and 3.8F, *piezo1*$^{11aa\ del/11aa\ del}$ mutant fish showed a significant reduction in the expression of osteoblast-specific genes. Together, these data confirm that *piezo1*$^{11aa\ del/11aa\ del}$ mutant fish showed low osteogenesis.

3.8 Progressive abnormalities in vertebral column of *piezo1*$^{11aa\ del/11aa\ del}$

Several studies have shown that adolescent idiopathic scoliosis can lead to intervertebral disc (IVD) degeneration in later life (Bertram et al., 2006;Hristova et al., 2011;Akazawa et al., 2017). Many of the abnormal bone features described, such as osteophyte formation, endplate sclerosis, facet joint changes, IVD narrowing, and ectopic calcification, have been observed in individuals with intervertebral disc degeneration.

To discern irregular bone alterations in the spine, a comparison was made between 3D-rendered micro-CT images of wildtype and mutant fish. Subsequently, an assessment was conducted to determine the frequency of abnormal bone characteristics observed in the spine. From this analysis, there were at least five abnormal bone features in *piezo1*$^{11aa\ del/11aa\ del}$ mutant fish at the age of 5 months, encompassing IVD calcification (IC), bone fusion (BF), ectopic bone calcification (EC), end-plate sclerosis (ES), and osteophytes (OP) (Figures 3.9A-F) (Kague et al., 2021).

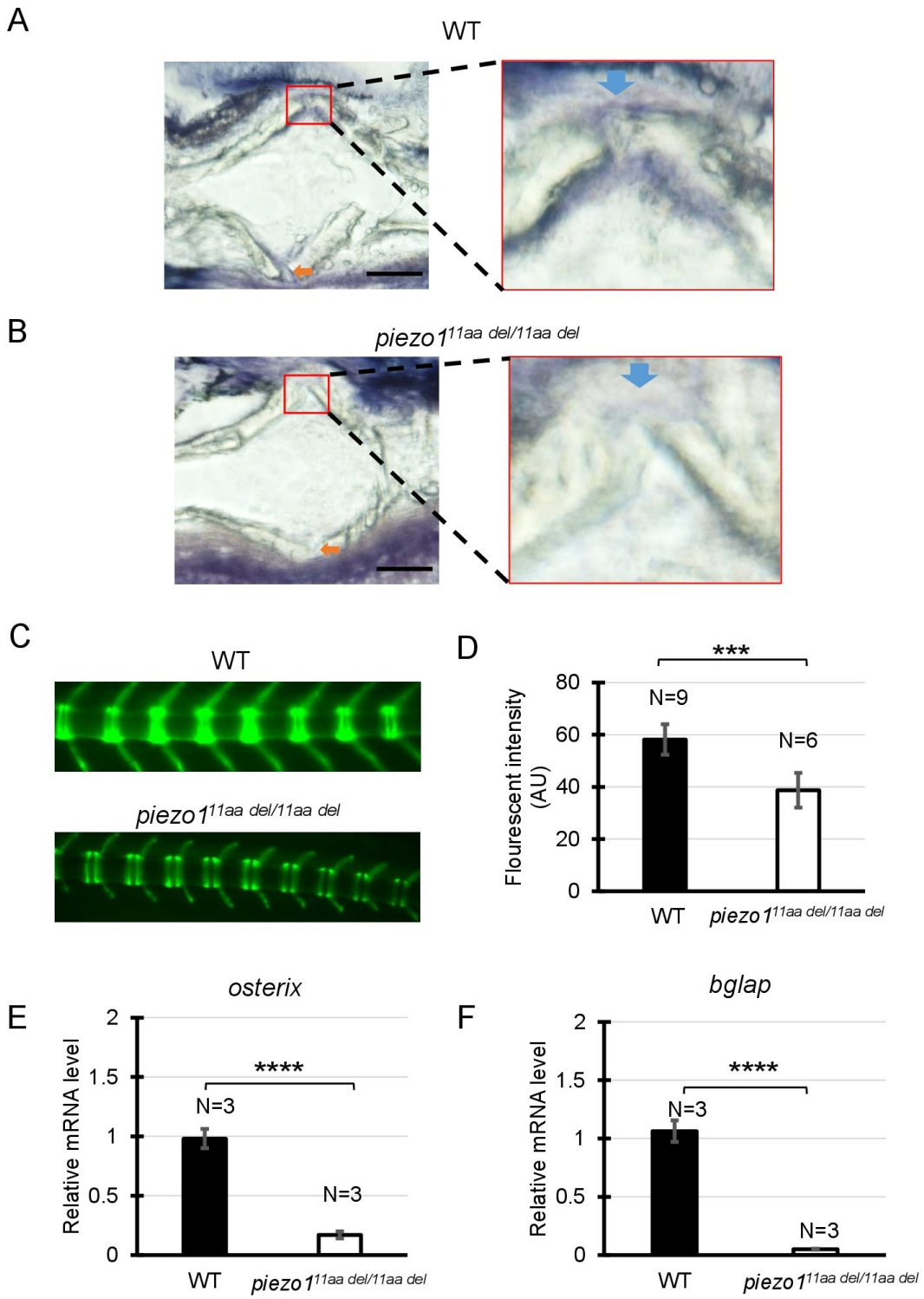

Figure 3.8 Abnormal osteoblast function. (A)(B) Representative image of alkaline phosphatase staining in vertebral bone section of wildtype (N=4) and *piezo1*$^{11aa\ del/11aa\ del}$ (N=5). Red boxes indicate the magnified area of growth plate. Blue arrow indicates center of growth plate, orange arrow indicates growth plate at the opposite site. Scale bar is 100 µm. (C) Fluorescence images of vertebral bone of wildtype;(*osx-GFP*) and *piezo1*$^{11aa\ del/11aa\ del}$; (*osx-GFP*) at 25 dpf. (D) Quantitative analysis of fluorescence area. Values are presented as mean ± SD and analyzed using student t-test. **** P < 0.001. mRNA level of (E) osterix, mid-stage osteoblast marker gene, and (F) osteoclacin/bglap, late-stage osteoblast marker gene.* Values are presented as mean ± SD and analyzed using student t-test. ***** P < 0.0001.*

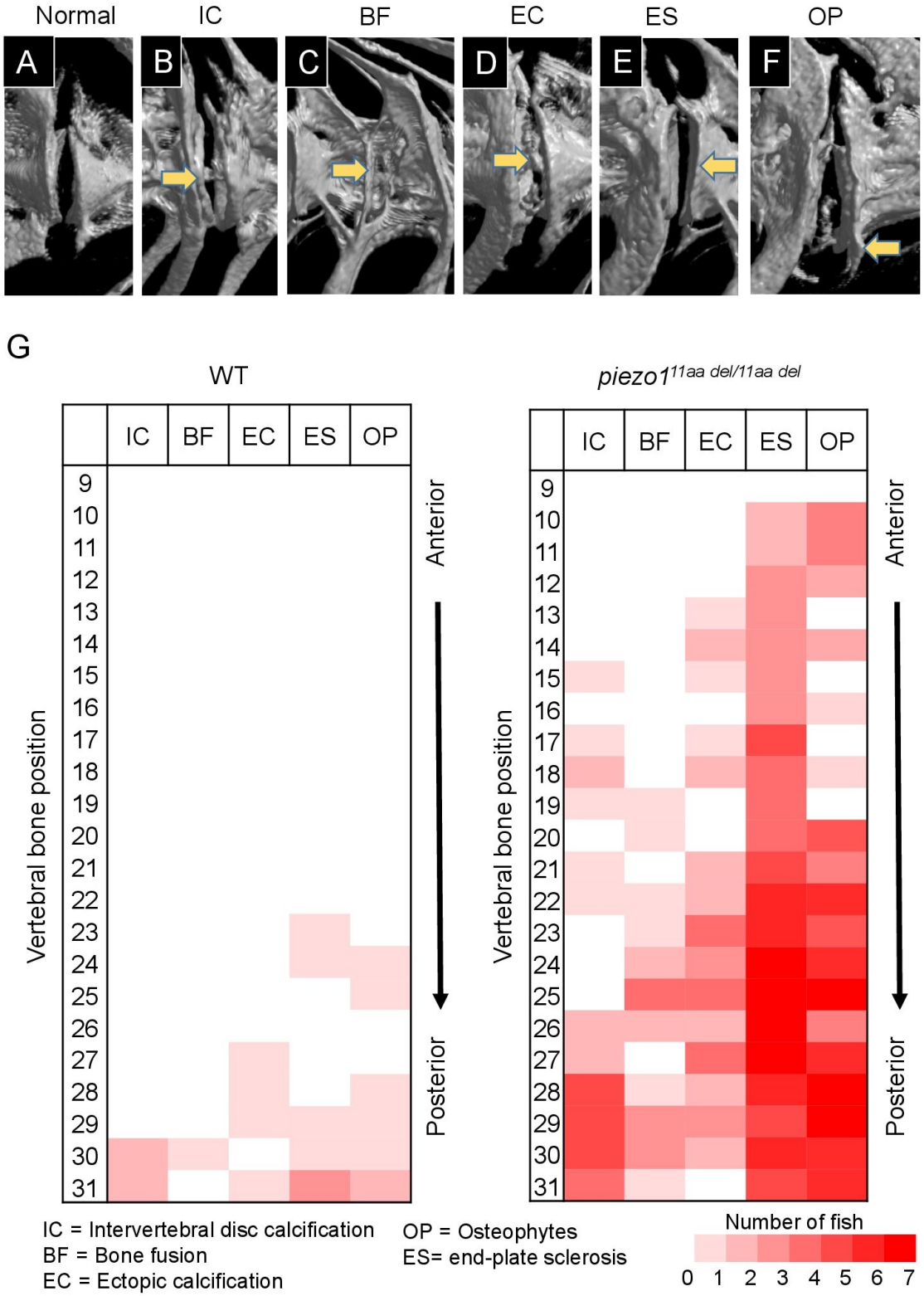

Figure 3.9 Abnormal changes of vertebral bone in *piezo1*$^{11aa\ del/11aa\ del}$. (A) Normal feature of bone; (B) Intervertebral disc calcification (IC); (C) Bone fusion (BF); (D) Ectopic calcification (EC); (E) End-plate sclerosis (ES); (F) Osteophytes formation (OP). (G) Heat map depicting the position and frequency of abnormal features of bone between wildtype and *piezo1*$^{11aa\ del/11aa\ del}$.

As shown in figure 3.9G, although had similar ages, bone abnormalities were more frequent in mutant than wildtype. This suggests *piezo1*$^{11aa\ del/11aa\ del}$ mutant fish might have premature bone degeneration. Malformation of vertebrae can occur at any site, regardless of the type of morphological abnormality, but are more frequent at sites close to the tail. Particularly distinct are the intervertebral calcification sites, with more than 80% occurring in the 28th to 30th vertebrae, where the physical stress from tail movement is expected to be greatest. This suggests that the cause of these bone abnormalities is mechanical stress.

3.9 Introducing functional *piezo1* gene into *piezo1* scoliosis mutant could develop normal spine

Identification of the causative cell is important for use as a disease model. The most likely candidate is osteoblasts, but since the *piezo1* gene is expressed in many tissues, Icannot rule out osteoblasts as the cause of the mutation in *piezo1*$^{11aa\ del/11aa\ del}$ mutant. Therefore, Iattempted to express *piezo1* using the osteoblast-specific promoter *sp7/osterix* to see if the mutation could be rescued (Figure 3.10A).

As expected, the phenotype variation of the mutant fish harboring transgene with the rescue plasmid were varied (Figure 3.10C). Although some small bones were slightly bent along the vertebrae, the reduced phenotype in the rescue mutant was confirmed in all of the TMD, Cobb angle, and percentage of bone with IVD calcifications (Figure 3.11A-7E).

This result confirms that the cells responsible for the bone morphological abnormalities in *piezo1* are osteoblasts. Furthermore, it shows that the severity of the morphological abnormality can be regulated by artificially altering the expression level of *piezo1*. This will increase the utility of the *piezo1*$^{11aa\ del/11aa\ del}$ fish as a pathological model.

3.10 Increase muscle mass could alleviate scoliosis symptoms

To evaluate the utility of *piezo1*$^{11aa\ del/11aa\ del}$ mutant fish as a model for pathology, it is necessary to determine whether the abnormal bone morphology of fish responds in the same manner as in humans to manipulations that aggravate or alleviate the symptoms of scoliosis. Scoliosis that develops during adolescence can sometimes be attributed to muscle defects (Lv et al., 2021). Furthermore, exercise, especially weight-bearing exercises that increase muscle mass, has been shown to be an effective treatment for scoliosis (Lau et al., 2021;Hui et al., 2022). Based on these facts, I hypothesized that increasing muscle mass might reduce scoliosis-like symptoms in *piezo1*$^{11aa\ del/11aa\ del}$ mutant fish. In fish and mice, inhibition of the *myostatin (mstnb)* gene, a protein that regulates muscle development (Welle et al., 2007;Suh et al., 2020) can increase muscle mass with little effect on other organs. Therefore, disrupting the *myostatin* gene in *piezo1*$^{11aa\ del/11aa\ del}$ fish can easily be used to study the relationship between muscle mass and the pathological level of scoliosis.

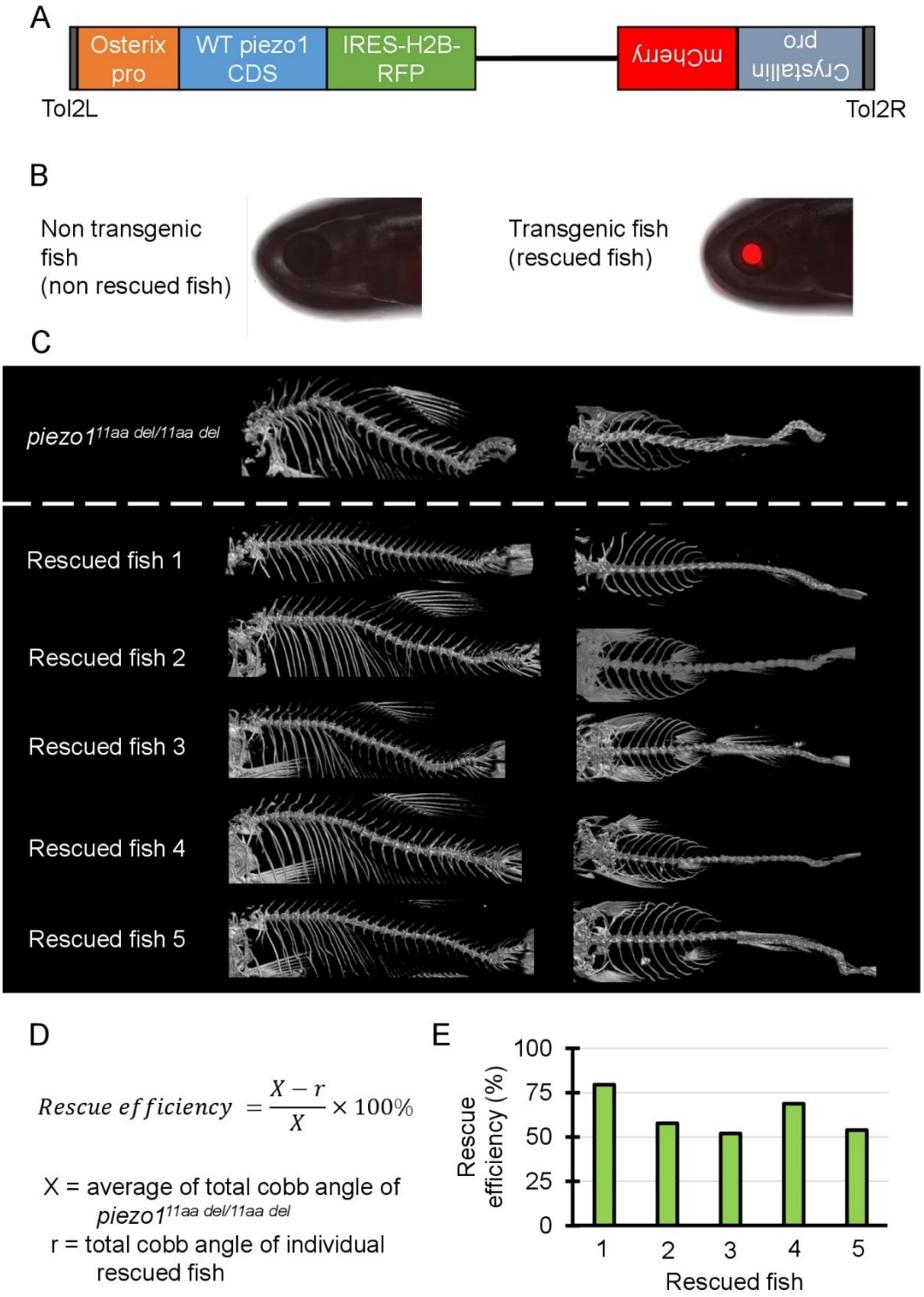

Figure 3.10 Validation of rescue experiment. (A) Schematic diagram of rescue plasmid. Notably, *sp7/osterix* promoter was used to express functional *piezo1* gene. (B) Confirmation of successful integration of rescue plasmid in zebrafish genome. Rescue plasmid has *crystallin-pro:mCherry*. Once the plasmid is expressed, red fluorescent will be emitted in eyes, indicating a transgenic fish. (C) Phenotype variation of rescued mutant fish. (D) Formula of measuring rescue efficiency. Introduction rescue plasmid in *piezo1*$^{11aa\ del/11aa\ del}$ alleviates scoliosis symptoms, but (E) the efficiency is varied among the rescue fish.

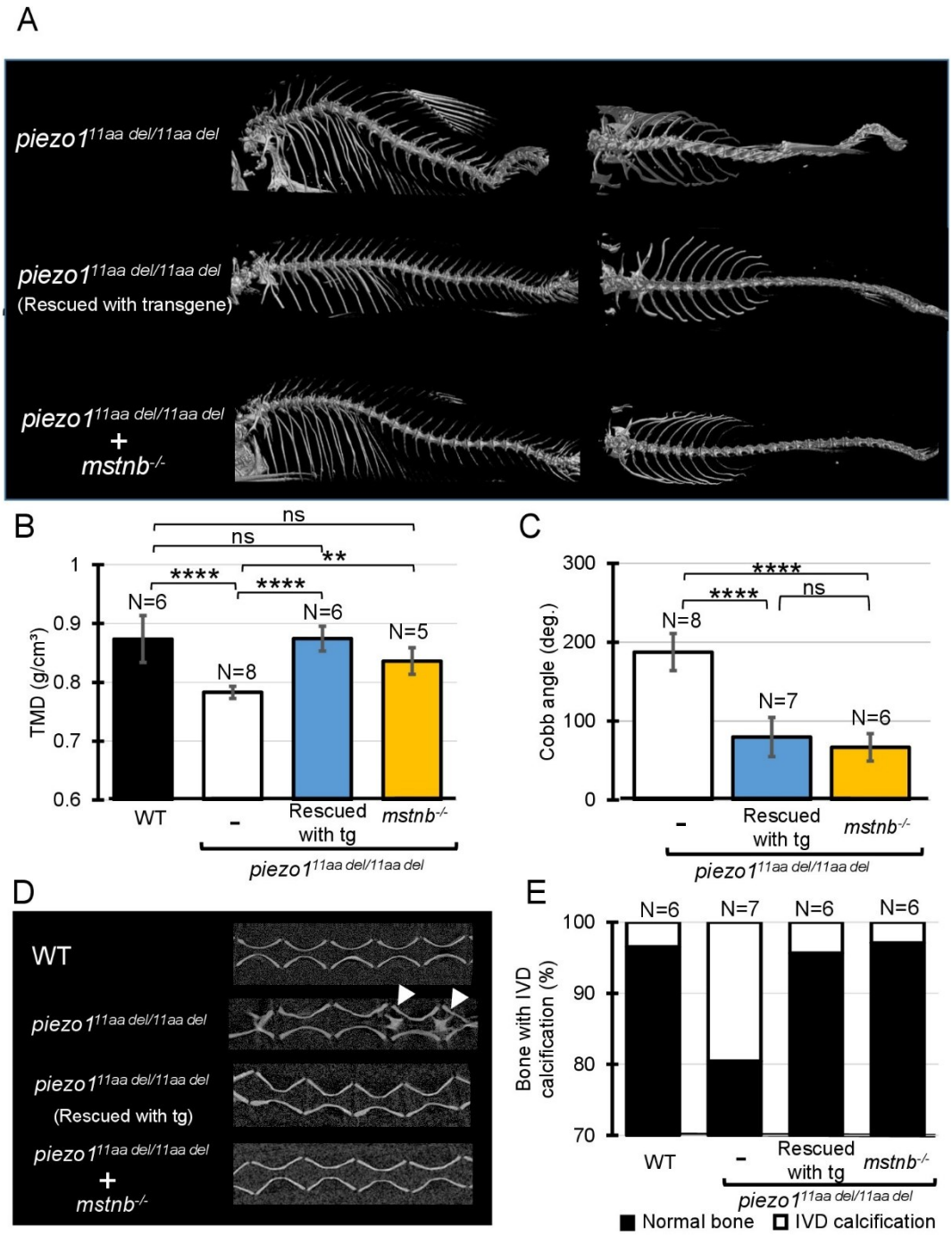

Figure 3.11 Introducing functional *piezo1* gene or increasing muscle mass can alleviate scoliosis symptoms**.** (A) Comparison of 3D reconstruction of micro-CT images. (B) Quantification of TMD from 5 individual segments of abdominal vertebrae of wildtype (N=6), *piezo1*$^{11aa\ del/11aa\ del}$ mutant (N=8), rescue mutant fish (N=6), and double mutant of *piezo1*$^{11aa\ del/11aa\ del}$; *mstnb*$^{-/-}$(N=5). (C) Combined Cobb angle of *piezo1*$^{11aa\ del/11aa\ del}$ mutant (N=8) rescue mutant fish (N=7), and double mutant of *piezo1*$^{11aa\ del/11aa\ del}$; *mstnb*$^{-/-}$ (N=6). (D) Sagittal section of the spine. Rescue mutant and *piezo1*$^{11aa\ del/11aa\ del}$; *mstnb*$^{-/-}$ have reduced the number of bone with IVD calcification (white arrows). (E) Graph depicting the percentage of bone with IVD calcification across bone segments 9 to 31. Values are presented as mean ± SD and analyzed using one-way ANOVA followed by Tukey's test. ns = non-significant; ** $P < 0.01$; *** $P < 0.001$; **** $P < 0.0001$

Using previously published guide RNA (Gao et al., 2016), zebrafish *myostatin* knockouts were produced by CRISPR/Cas9. Zebrafish *mstnb*$^{-/-}$ exhibited relatively larger body size compared to wildtype (Gao et al., 2016), with a clear increase in muscle mass around the spine (Supplementary Figure S8). Next, *myostatin* knockout zebrafish were crossed twice with *piezo1*$^{11aa\ del/+}$ to examine the relationship between increased muscle mass and scoliosis severity. Figure 3.11 shows an overview of the vertebrae and the statistical data. As expected, the strength of the spinal curvature decreased with increasing muscle (Figure 3.11A), and tissue mineral density increased (Figure 3.11B). When quantified in terms of Cobb angle, it decreased to almost 30% (Figure 3.11C). Also, abnormal calcification in the intervertebral disc (IVD) region was also barely observed (Figure 3.11D, 3.11F). This suggests a decrease in bone degeneration. These findings are strong evidence that increasing muscle mass alleviates scoliosis and promotes bone formation, suggesting a potential therapeutic approach for the treatment of scoliosis. *piezo1*$^{11aa\ del/11aa\ del}$ fish may be used effectively as a pathological model for scoliosis. I suggest that *piezo1*$^{11aa\ del/11aa\ del}$ fish is a good model for the treatment of scoliosis, as they have been shown to be able to increase the muscle mass of the spine and to increase the bone mineral density of the spine.

Chapter 4

4. Discussion and Conclusion

Scoliosis is a disease caused by the almost unique posture of humans in the vertebrate world, in which they stand upright on two legs, and it has been difficult to obtain an experimental system that can serve as a model for the disease (Castelein et al., 2005;Bobyn et al., 2015;Xie et al., 2022). On the other hand, there have been cases of scoliosis-like symptoms in fish (Gorman et al., 2007;Gorman and Breden, 2009), and it is thought that the longitudinal compression of the spine caused by the propulsive force of the caudal fin is similar to that caused by the upright posture in humans (Figure 4.1).

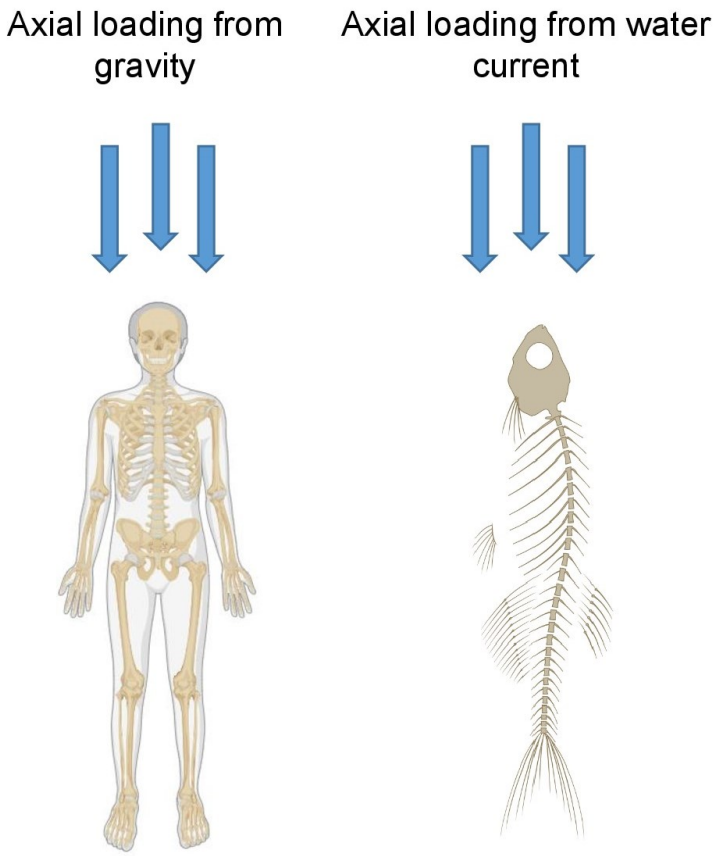

Figure 4.1 Similarities of biomechanical forces between human and fish

We have established a pathological model of scoliosis in zebrafish by manipulating the *piezo* genes, which are mechanotropic stimulus receptors in the cells. Zebrafish have two *piezo* genes (*piezo1* and *piezo2a*) involved in bone formation. When both genes were knocked out, various abnormalities including bone formation appeared in early development and early death occurred. However, an in-frame mutation in the *piezo1* gene (11 amino acid deletion) was not lethal and caused morphological abnormalities of the spine similar to scoliosis in humans. The fact that the morphological abnormalities occur later in life and that bone density is reduced, also suggests that the zebrafish spinal morphology may be homologous to human scoliosis. Since zebrafish can be easily bred in large numbers and genetic manipulation tools have been

developed, it is expected that mutant zebrafish will be used to study the pathogenesis of scoliosis and to screen for therapeutic agents.

4.1 Usefulness as a pathological model

The pathological model of scoliosis created in this study using zebrafish has several advantages besides the ease of rearing a large number of animals. As shown in figure 7, the severity of the disease can be modulated by the expression of normal *piezo1* and *piezo2a* genes. This could be a useful property when screening for therapies. When screening for therapeutic agents, it is expected that if the severity of the model is too strong, the effect will not be apparent, and if the severity is too weak, the data may be unstable. Screening for individuals of varying severity would reduce the likelihood of missing an effective drug. Another advantage is the ability to test the efficacy of treatments other than relaxing agents, such as physical therapy, as in the present study, where muscle augmentation due to deletion of the *myostatin* gene induced a resolution of symptoms. A more advanced approach would be to investigate the relationship between exercise therapy and scoliosis, such as artificially inducing muscle contraction with light. Briefly, the similarities between human idiopathic scoliosis and piezo1 scoliosis mutant can be seen in table 4.1

Table 4.1 Similarity aspect between human idiopathic scoliosis and *piezo1*$^{11aa\ del/11aa\ del}$ scoliosis mutant fish

Parameter	Human idiopathic scoliosis	Piezo1 idiopathic Scoliosis model
Occurs during adolescent period	Yes (Konieczny et al., 2013)	Yes
Osteopenia (reduce BMD)	Yes (Sarioglu et al., 2019;Li et al., 2020;Almomen et al., 2021)	Yes
Spinal column asymmetric	Yes (Shea et al., 2004;Schlager et al., 2018)	Yes
Progressive bone abnormality	Yes (Bertram et al., 2006;Hristova et al., 2011;Akazawa et al., 2017)	Yes

4.2 Causal relationship between scoliosis and osteoporosis

Although scoliosis and osteoporosis are distinct skeletal conditions with separate sets of symptoms and underlying causes, there is a suggested connection between them. Numerous clinical reports have indicated that individuals with idiopathic scoliosis often exhibit lower bone mineral density (BMD) (Li et al., 2008;Sadat-Ali et al., 2008;Nishida et al., 2023;Wu et al., 2023), a key indicator of osteoporosis. Similar to these studies, I also found remarkably lower BMD values in *piezo1*$^{11aa\ del/11aa\ del}$ mutant compared to siblings. However, it remains unclear whether osteoporosis plays a causative role or is a consequence of scoliosis.

Based on current knowledge, it is plausible that osteoporosis may be an underlying factor contributing to the development of scoliosis. Histological examinations of trabecular bone in idiopathic scoliosis patients have shown decreased osteoblast activity (Cheng et al., 2001). Additionally, children diagnosed with idiopathic scoliosis have demonstrated diminished osteogenic differentiation potential in their mesenchymal stem cells (Park et al., 2009;Chen et al., 2016). These findings suggest that the decline in osteoblast activity, leading to a reduction in BMD, may occur prior to the formation of lateral spinal curvature. Low bone density

resulting from abnormal osteogenic activity could increase the risk of bone fractures. The presence of microfractures may, in turn, contribute to bone asymmetry, potentially exacerbated by axial loading. Eventually, this leads to the development of spinal deformity in a cyclical and interdependent manner.

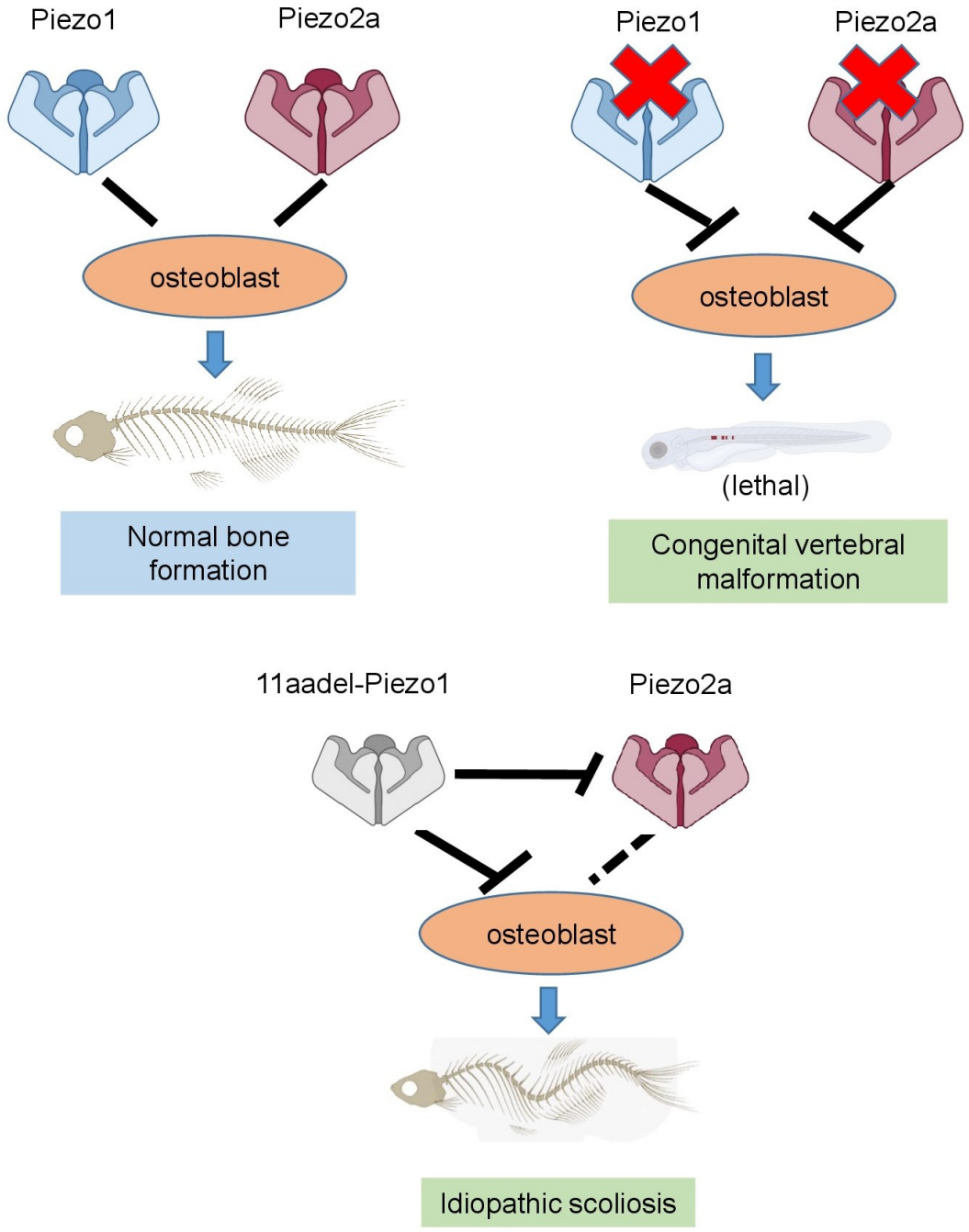

Figure 4.2 Schematic model of Piezo1 and Piezo2a channel function in bone formation in Zebrafish

4.3 *piezo1* and *piezo2a* might have overlapping function

In my first finding, I demonstrated that the homozygous single mutant lacking *piezo1* or *piezo2a* was viable, fertile, and did not show any developmental defect, especially in bone. Relative mRNA expression of *piezo1* and *piezo2a* in each mutant background did not change significantly, indicating transcriptional adaptation or NMD pathway is not recruited for the mechanism of genetic buffering (El-Brolosy and Stainier, 2017).

Instead of relying on transcriptional adaptation, the most likely explanation for genetic compensation in the *piezo1* null mutant is gene redundancy. This concept suggests that the loss of one gene may be compensated by another gene with overlapping functions and expression patterns(El-Brolosy and Stainier, 2017). It has been reported that *piezo1* and *piezo2a* exhibit similar expression patterns (Faucherre et al., 2013). Moreover, double knock-out mutant died after 10 dpf, while mutant harbouring at least one wildtype allele of *piezo1* or *piezo2a* (*piezo1*$^{-/-}$*;piezo2a*$^{+/-}$ or *piezo1*$^{+/-}$*;piezo2a*$^{-/-}$) showed normal phenotype and could reach adult stage. This indicates that at least one functional gene either *piezo1* or *piezo2a* is enough for normal development of zebrafish, supporting the result of gene compensation through redundant function of *piezo1* or *piezo2a* gene. Figure 4.2 shows a schematic model of how Piezo1 and Piezo2a channels function in zebrafish bone formation.

4.4 *piezo1*$^{11aa\ del/11aa\ del}$ mutant for a tool to investigate the *piezo* genes in other cells

piezo1 and *piezo2a* are homologous in function and both genes are expressed in almost all cells. Double deletion mutations cause hypoplasia in bladder and body segments as well as osteogenesis imperfecta. These results indicate that the *piezo* genes are also essential for the formation of other organs in zebrafish and are consistent with other reports showing *piezo* gene function in a variety of cells. Although 11aa del-Piezo1 is a mutation in the *piezo1* gene, it is also possible this can reduce the function of *piezo2a* with a dominant-negative effect through heteromeric channel formation (Gnanasambandam et al., 2018). This also consistent with mosaic mutant experiment (Figure 1J) when *piezo2a* function was partially reduced. This feature may allow *in vivo* studies of *piezo* genes' function in other cells. Specifically, expression of the 11aa del-Piezo1 mutant gene using a target cell-specific promoter would avoid lethality and reveal the role of the *piezo* genes in those cells.

Bibliography

Akazawa, T., Kotani, T., Sakuma, T., Minami, S., Orita, S., Fujimoto, K., Shiga, Y., Takaso, M., Inoue, G., Miyagi, M., Aoki, Y., Niki, H., Torii, Y., Morioka, S., Ohtori, S., and Takahashi, K. (2017). Spinal fusion on adolescent idiopathic scoliosis patients with the level of L4 or lower can increase lumbar disc degeneration with sagittal imbalance 35 years after surgery. *Spine Surg Relat Res* 1**,** 72-77.

Almomen, F.A., Altaweel, A.M., Abunadi, A.K., Hashem, A.E., Alqarni, R.M., and Alsiddiky, A.M. (2021). Determining the correlation between Cobb angle severity and bone mineral density in women with adolescent idiopathic scoliosis. *J Taibah Univ Med Sci* 16**,** 365-368.

Arnadóttir, J., and Chalfie, M. (2010). Eukaryotic mechanosensitive channels. *Annu Rev Biophys* 39**,** 111-137.

Assaraf, E., Blecher, R., Heinemann-Yerushalmi, L., Krief, S., Carmel Vinestock, R., Biton, I.E., Brumfeld, V., Rotkopf, R., Avisar, E., Agar, G., and Zelzer, E. (2020). Piezo2 expressed in proprioceptive neurons is essential for skeletal integrity. *Nat Commun* 11**,** 3168.

Bae, C., Sachs, F., and Gottlieb, P.A. (2011). The mechanosensitive ion channel Piezo1 is inhibited by the peptide GsMTx4. *Biochemistry* 50**,** 6295-6300.

Bagwell, J., Norman, J., Ellis, K., Peskin, B., Hwang, J., Ge, X., Nguyen, S.V., Mcmenamin, S.K., Stainier, D.Y., and Bagnat, M. (2020). Notochord vacuoles absorb compressive bone growth during zebrafish spine formation. *Elife* 9.

Bearce, E.A., Irons, Z.H., O'hara-Smith, J.R., Kuhns, C.J., Fisher, S.I., Crow, W.E., and Grimes, D.T. (2022). Urotensin II-related peptides, Urp1 and Urp2, control zebrafish spine morphology. *Elife* 11.

Bertram, H., Steck, E., Zimmerman, G., Chen, B., Carstens, C., Nerlich, A., and Richter, W. (2006). Accelerated intervertebral disc degeneration in scoliosis versus physiological ageing develops against a background of enhanced anabolic gene expression. *Biochem Biophys Res Commun* 342**,** 963-972.

Bobyn, J.D., Little, D.G., Gray, R., and Schindeler, A. (2015). Animal models of scoliosis. *J Orthop Res* 33**,** 458-467.

Brohawn, S.G., Campbell, E.B., and Mackinnon, R. (2014). Physical mechanism for gating and mechanosensitivity of the human TRAAK K+ channel. *Nature* 516**,** 126-130.

Buglo, E., Sarmiento, E., Martuscelli, N.B., Sant, D.W., Danzi, M.C., Abrams, A.J., Dallman, J.E., and Züchner, S. (2020). Genetic compensation in a stable slc25a46 mutant zebrafish: A case for using F0 CRISPR mutagenesis to study phenotypes caused by inherited disease. *PLoS One* 15**,** e0230566.

Bulman, M.P., Kusumi, K., Frayling, T.M., Mckeown, C., Garrett, C., Lander, E.S., Krumlauf, R., Hattersley, A.T., Ellard, S., and Turnpenny, P.D. (2000). Mutations in the human delta homologue, DLL3, cause axial skeletal defects in spondylocostal dysostosis. *Nat Genet* 24**,** 438-441.

Burwell, R.G., Aujla, R.K., Grevitt, M.P., Dangerfield, P.H., Moulton, A., Randell, T.L., and Anderson, S.I. (2009). Pathogenesis of adolescent idiopathic scoliosis in girls - a double neuro-osseous theory involving disharmony between two nervous systems, somatic and autonomic expressed in the spine and trunk: possible dependency on sympathetic nervous system and hormones with implications for medical therapy. *Scoliosis* 4**,** 24.

Castelein, R.M., Van Dieën, J.H., and Smit, T.H. (2005). The role of dorsal shear forces in the pathogenesis of adolescent idiopathic scoliosis--a hypothesis. *Med Hypotheses* 65**,** 501-508.

Chen, C., Xu, C., Zhou, T., Gao, B., Zhou, H., Zhang, C., Huang, D., and Su, P. (2016). Abnormal osteogenic and chondrogenic differentiation of human mesenchymal stem cells from patients with adolescent idiopathic scoliosis in response to melatonin. *Mol Med Rep* 14**,** 1201-1209.

Chen, F., Sun, M., Peng, F., Lai, Y., Jiang, Z., Zhang, W., Li, T., and Jing, X. (2023). Compressive stress induces spinal vertebral growth plate chondrocytes apoptosis via Piezo1. *J Orthop Res* 41**,** 1792-1802.

Cheng, J.C., Castelein, R.M., Chu, W.C., Danielsson, A.J., Dobbs, M.B., Grivas, T.B., Gurnett, C.A., Luk, K.D., Moreau, A., Newton, P.O., Stokes, I.A., Weinstein, S.L., and Burwell, R.G. (2015). Adolescent idiopathic scoliosis. *Nat Rev Dis Primers* 1**,** 15030.

Cheng, J.C., Tang, S.P., Guo, X., Chan, C.W., and Qin, L. (2001). Osteopenia in adolescent idiopathic scoliosis: a histomorphometric study. *Spine (Phila Pa 1976)* 26**,** E19-23.

Chung, L.Y., Nam, H.K., Rhie, Y.J., Huh, R., and Lee, K.H. (2020). Prevalence of idiopathic scoliosis in girls with central precocious puberty: effect of a gonadotropin-releasing hormone agonist. *Ann Pediatr Endocrinol Metab* 25**,** 92-96.

Coste, B., Mathur, J., Schmidt, M., Earley, T.J., Ranade, S., Petrus, M.J., Dubin, A.E., and Patapoutian, A. (2010). Piezo1 and Piezo2 are essential components of distinct mechanically activated cation channels. *Science* 330**,** 55-60.

Cox, C.D., Bavi, N., and Martinac, B. (2019). Biophysical Principles of Ion-Channel-Mediated Mechanosensory Transduction. *Cell Rep* 29**,** 1-12.

Crispino, M., Crispino, E. (2015). Spine. In: Olivetti, L. (eds) Atlas of Imaging Anatomy. Springer, Cham. https://doi.org/10.1007/978-3-319-10750-9_2

El-Brolosy, M.A., and Stainier, D.Y.R. (2017). Genetic compensation: A phenomenon in search of mechanisms. *PLoS Genet* 13**,** e1006780.

Faucherre, A., Nargeot, J., Mangoni, M.E., and Jopling, C. (2013). piezo2b regulates vertebrate light touch response. *J Neurosci* 33**,** 17089-17094.

Gao, Y., Dai, Z., Shi, C., Zhai, G., Jin, X., He, J., Lou, Q., and Yin, Z. (2016). Depletion of Myostatin b Promotes Somatic Growth and Lipid Metabolism in Zebrafish. *Front Endocrinol (Lausanne)* 7**,** 88.

Gnanasambandam, R., Bae, C., Ziegler, L., Sachs, F., and Gottlieb, P.A. (2018). Functional analyses of heteromeric human PIEZO1 Channels. *PLoS One* 13**,** e0207309.

Gorman, K.F., and Breden, F. (2009). Idiopathic-type scoliosis is not exclusive to bipedalism. *Med Hypotheses* 72**,** 348-352.

Gorman, K.F., Tredwell, S.J., and Breden, F. (2007). The mutant guppy syndrome curveback as a model for human heritable spinal curvature. *Spine (Phila Pa 1976)* 32**,** 735-741.

Grimes, D.T., Boswell, C.W., Morante, N.F., Henkelman, R.M., Burdine, R.D., and Ciruna, B. (2016). Zebrafish models of idiopathic scoliosis link cerebrospinal fluid flow defects to spine curvature. *Science* 352**,** 1341-1344.

Gudipaty, S.A., Lindblom, J., Loftus, P.D., Redd, M.J., Edes, K., Davey, C.F., Krishnegowda, V., and Rosenblatt, J. (2017). Mechanical stretch triggers rapid epithelial cell division through Piezo1. *Nature* 543**,** 118-121.

Guido, G., Scaglione, M., Fabbri, L., and Ceglia, M.J. (2009). The "osteoporosis disease". *Clin Cases Miner Bone Metab* 6**,** 114-116.

Haelterman, N., and Lim, J. (2019). Sensing the load. *Elife* 8.

Haliloglu, G., Becker, K., Temucin, C., Talim, B., Küçükşahin, N., Pergande, M., Motameny, S., Nürnberg, P., Aydingoz, U., Topaloglu, H., and Cirak, S. (2017). Recessive PIEZO2 stop mutation causes distal arthrogryposis with distal muscle weakness, scoliosis and proprioception defects. *J Hum Genet* 62**,** 497-501.

Harrell, K.M., Dudek, R. Lippincott®Illustrated Reviews: Anatomy. Philadelphia, Walters Kluwer. 2019.

Hayes, M., Gao, X., Yu, L.X., Paria, N., Henkelman, R.M., Wise, C.A., and Ciruna, B. (2014). ptk7 mutant zebrafish models of congenital and idiopathic scoliosis implicate dysregulated Wnt signalling in disease. *Nat Commun* 5**,** 4777.

Hristova, G.I., Jarzem, P., Ouellet, J.A., Roughley, P.J., Epure, L.M., Antoniou, J., and Mwale, F. (2011). Calcification in human intervertebral disc degeneration and scoliosis. *J Orthop Res* 29**,** 1888-1895.

Hui, S.S.C., Lau, R.W.L., Cheng, J.C.Y., and Lam, T.P. (2022). High-impact weight-bearing home exercises in girls with adolescent idiopathic scoliosis: a pilot study (abridged secondary publication). *Hong Kong Med J* 28 Suppl 3**,** 31-33.

Iwasaki, M., Kuroda, J., Kawakami, K., and Wada, H. (2018). Epidermal regulation of bone morphogenesis through the development and regeneration of osteoblasts in the zebrafish scale. *Dev Biol* 437**,** 105-119.

Kague, E., Turci, F., Newman, E., Yang, Y., Brown, K.R., Aglan, M.S., Otaify, G.A., Temtamy, S.A., Ruiz-Perez, V.L., Cross, S., Royall, C.P., Witten, P.E., and Hammond, C.L. (2021). 3D assessment of intervertebral disc degeneration in zebrafish identifies changes in bone density that prime disc disease. *Bone Res* 9**,** 39.

Kawakami, K., Shima, A., and Kawakami, N. (2000). Identification of a functional transposase of the Tol2 element, an Ac-like element from the Japanese medaka fish, and its transposition in the zebrafish germ lineage. *Proc Natl Acad Sci U S A* 97**,** 11403-11408.

Kawamoto, T. (2003). Use of a new adhesive film for the preparation of multi-purpose fresh-frozen sections from hard tissues, whole-animals, insects and plants. *Arch Histol Cytol* 66**,** 123-143.

Konieczny, M.R., Senyurt, H., and Krauspe, R. (2013). Epidemiology of adolescent idiopathic scoliosis. *J Child Orthop* 7**,** 3-9.

Kulis, A., Goździalska, A., Drąg, J., Jaśkiewicz, J., Knapik-Czajka, M., Lipik, E., and Zarzycki, D. (2015). Participation of sex hormones in multifactorial pathogenesis of adolescent idiopathic scoliosis. *Int Orthop* 39**,** 1227-1236.

Lau, R.W., Cheuk, K.Y., Ng, B.K., Tam, E.M., Hung, A.L., Cheng, J.C., Hui, S.S., and Lam, T.P. (2021). Effects of a Home-Based Exercise Intervention (E-Fit) on Bone Density, Muscle Function, and Quality of Life in Girls with Adolescent Idiopathic Scoliosis (AIS): A Pilot Randomized Controlled Trial. *Int J Environ Res Public Health* 18.

Lee, S., Park, S., Kim, H.Y., Chae, J.H., and Ko, J.M. (2021). Extended phenotypes of PIEZO1-related lymphatic dysplasia caused by two novel compound heterozygous variants. *Eur J Med Genet* 64**,** 104295.

Li, L., Krantz, I.D., Deng, Y., Genin, A., Banta, A.B., Collins, C.C., Qi, M., Trask, B.J., Kuo, W.L., Cochran, J., Costa, T., Pierpont, M.E., Rand, E.B., Piccoli, D.A., Hood, L., and Spinner, N.B. (1997). Alagille syndrome is caused by mutations in human Jagged1, which encodes a ligand for Notch1. *Nat Genet* 16**,** 243-251.

Li, X., Han, L., Nookaew, I., Mannen, E., Silva, M.J., Almeida, M., and Xiong, J. (2019). Stimulation of Piezo1 by mechanical signals promotes bone anabolism. *Elife* 8.

Li, X., Hung, V.W.Y., Yu, F.W.P., Hung, A.L.H., Ng, B.K.W., Cheng, J.C.Y., Lam, T.P., and Yip, B.H.K. (2020). Persistent low-normal bone mineral density in adolescent idiopathic scoliosis with different curve severity: A longitudinal study from presentation to beyond skeletal maturity and peak bone mass. *Bone* 133**,** 115217.

Li, X.F., Li, H., Liu, Z.D., and Dai, L.Y. (2008). Low bone mineral status in adolescent idiopathic scoliosis. *Eur Spine J* 17**,** 1431-1440.

Lu, W.W., Hu, Y., Luk, K.D., Cheung, K.M., and Leong, J.C. (2002). Paraspinal muscle activities of patients with scoliosis after spine fusion: an electromyographic study. *Spine (Phila Pa 1976)* 27**,** 1180-1185.

Lv, X., Xu, J., Jiang, J., Wu, P., Tan, R., and Wang, B. (2021). Genetic animal models of scoliosis: A systematical review. *Bone* 152**,** 116075.

Marie-Hardy, L., Cantaut-Belarif, Y., Pietton, R., Slimani, L., and Pascal-Moussellard, H. (2021). Author Correction: The orthopedic characterization of cfap298. *Sci Rep* 11**,** 16017.

Marshall, K.L., and Lumpkin, E.A. (2012). The molecular basis of mechanosensory transduction. *Adv Exp Med Biol* 739**,** 142-155.

Martinac, B., and Poole, K. (2018). Mechanically activated ion channels. *Int J Biochem Cell Biol* 97**,** 104-107.

Murthy, S.E., Dubin, A.E., and Patapoutian, A. (2017). Piezos thrive under pressure: mechanically activated ion channels in health and disease. *Nat Rev Mol Cell Biol* 18**,** 771-783.

Nishida, M., Yagi, M., Suzuki, S., Takahashi, Y., Nori, S., Tsuji, O., Nagoshi, N., Fujita, N., Matsumoto, M., Nakamura, M., and Watanabe, K. (2023). Persistent low bone mineral density in adolescent idiopathic scoliosis: A longitudinal study. *J Orthop Sci* 28**,** 1099-1104.

Nourse, J.L., and Pathak, M.M. (2017). How cells channel their stress: Interplay between Piezo1 and the cytoskeleton. *Semin Cell Dev Biol* 71**,** 3-12.

Panjabi MM. The stabilizing system of the spine. Part I. Function, dysfunction, adaptation, and enhancement. *J Spinal Disord*. 1992 Dec;5(4):383-9; discussion 397. doi: 10.1097/00002517-199212000-00001. PMID: 1490034.

Park, W.W., Suh, K.T., Kim, J.I., Kim, S.J., and Lee, J.S. (2009). Decreased osteogenic differentiation of mesenchymal stem cells and reduced bone mineral density in patients with adolescent idiopathic scoliosis. *Eur Spine J* 18**,** 1920-1926.

Parpaite, T., and Coste, B. (2017). Piezo channels. *Curr Biol* 27**,** R250-R252.

Raisz, L.G. (1999). Prostaglandins and bone: physiology and pathophysiology. *Osteoarthritis Cartilage* 7**,** 419-421.

Ran, F.A., Hsu, P.D., Wright, J., Agarwala, V., Scott, D.A., and Zhang, F. (2013). Genome engineering using the CRISPR-Cas9 system. *Nat Protoc* 8**,** 2281-2308.

Renn, J., and Winkler, C. (2009). Osterix-mCherry transgenic medaka for in vivo imaging of bone formation. *Dev Dyn* 238**,** 241-248.

Sadat-Ali, M., Al-Othman, A., Bubshait, D., and Al-Dakheel, D. (2008). Does scoliosis causes low bone mass? A comparative study between siblings. *Eur Spine J* 17**,** 944-947.

Sarioglu, O., Gezer, S., Sarioglu, F.C., Koremezli, N., Kara, T., Akcali, O., Ozaksoy, D., and Balci, A. (2019). Evaluation of vertebral bone mineral density in scoliosis by using quantitative computed tomography. *Pol J Radiol* 84**,** e131-e135.

Scaal M. Early development of the vertebral column. Semin Cell Dev Biol. 2016 Jan;49:83-91. doi: 10.1016/j.semcdb.2015.11.003. Epub 2015 Nov 10. PMID: 26564689.

Schlager, B., Krump, F., Boettinger, J., Niemeyer, F., Ruf, M., Kleiner, S., Beer, M., and Wilke, H.J. (2018). Characteristic morphological patterns within adolescent idiopathic scoliosis may be explained by mechanical loading. *Eur Spine J* 27**,** 2184-2191.

She, J., Wu, Y., Lou, B., Lodd, E., Klems, A., Schmoehl, F., Yuan, Z., Noble, F.L., and Kroll, J. (2019). Genetic compensation by. *Cell Cycle* 18**,** 2683-2696.

Shea, K.G., Ford, T., Bloebaum, R.D., D'astous, J., and King, H. (2004). A comparison of the microarchitectural bone adaptations of the concave and convex thoracic spinal facets in idiopathic scoliosis. *J Bone Joint Surg Am* 86**,** 1000-1006.

Stokes, I.A., Burwell, R.G., Dangerfield, P.H., and Ibse (2006). Biomechanical spinal growth modulation and progressive adolescent scoliosis--a test of the 'vicious cycle' pathogenetic hypothesis: summary of an electronic focus group debate of the IBSE. *Scoliosis* 1**,** 16.

Sugisawa, E., Takayama, Y., Takemura, N., Kondo, T., Hatakeyama, S., Kumagai, Y., Sunagawa, M., Tominaga, M., and Maruyama, K. (2020). RNA Sensing by Gut Piezo1 Is Essential for Systemic Serotonin Synthesis. *Cell* 182**,** 609-624.e621.

Suh, J., Kim, N.K., Lee, S.H., Eom, J.H., Lee, Y., Park, J.C., Woo, K.M., Baek, J.H., Kim, J.E., Ryoo, H.M., Lee, S.J., and Lee, Y.S. (2020). GDF11 promotes osteogenesis as opposed to MSTN, and follistatin, a MSTN/GDF11 inhibitor, increases muscle mass but weakens bone. *Proc Natl Acad Sci U S A* 117**,** 4910-4920.

Sun, W., Chi, S., Li, Y., Ling, S., Tan, Y., Xu, Y., Jiang, F., Li, J., Liu, C., Zhong, G., Cao, D., Jin, X., Zhao, D., Gao, X., Liu, Z., and Xiao, B. (2019). The mechanosensitive Piezo1 channel is required for bone formation. *Elife* 8.

Syeda, R., Florendo, M.N., Cox, C.D., Kefauver, J.M., Santos, J.S., Martinac, B., and Patapoutian, A. (2016). Piezo1 Channels Are Inherently Mechanosensitive. *Cell Rep* 17**,** 1739-1746.

Syeda, R., Xu, J., Dubin, A.E., Coste, B., Mathur, J., Huynh, T., Matzen, J., Lao, J., Tully, D.C., Engels, I.H., Petrassi, H.M., Schumacher, A.M., Montal, M., Bandell, M., and Patapoutian, A. (2015). Chemical activation of the mechanotransduction channel Piezo1. *Elife* 4.

Studnicka K, Ampat G. Lumbar Stabilization. [Updated 2023 Aug 14]. In: *StatPearls* [Internet]. Treasure Island (FL): StatPearls Publishing; 2024 Jan-. Available from: https://www.ncbi.nlm.nih.gov/books/NBK562179/

Tominari, T., Ichimaru, R., Taniguchi, K., Yumoto, A., Shirakawa, M., Matsumoto, C., Watanabe, K., Hirata, M., Itoh, Y., Shiba, D., Miyaura, C., and Inada, M. (2019). Hypergravity and microgravity exhibited reversal effects on the bone and muscle mass in mice. *Sci Rep* 9**,** 6614.

Turnquist, J. E., & Minugh-Purvis, N. (2012). Functional morphology. In *Nonhuman primates in biomedical research: Biology and management* (pp. 87–129). London, UK: Academic Press.

Tong, X., Chen, X., Zhang, S., Huang, M., Shen, X., Xu, J., and Zou, J. (2019). The Effect of Exercise on the Prevention of Osteoporosis and Bone Angiogenesis. *Biomed Res Int* 2019**,** 8171897.

Troutwine, B.R., Gontarz, P., Konjikusic, M.J., Minowa, R., Monstad-Rios, A., Sepich, D.S., Kwon, R.Y., Solnica-Krezel, L., and Gray, R.S. (2020). The Reissner Fiber Is Highly Dynamic In Vivo and Controls Morphogenesis of the Spine. *Curr Biol* 30**,** 2353-2362.e2353.

Uehara, M., Kosho, T., Takano, K., Inaba, Y., Kuraishi, S., Ikegami, S., Oba, H., Takizawa, T., Munakata, R., Hatakenaka, T., and Takahashi, J. (2020). Proximal Junctional Kyphosis After Posterior Spinal Fusion for Severe Kyphoscoliosis in a Patient With PIEZO2-deficient Arthrogryposis Syndrome. *Spine (Phila Pa 1976)* 45**,** E600-E604.

Welle, S., Bhatt, K., Pinkert, C.A., Tawil, R., and Thornton, C.A. (2007). Muscle growth after postdevelopmental myostatin gene knockout. *Am J Physiol Endocrinol Metab* 292**,** E985-991.

Whittle, J., Antunes, L., Harris, M., Upshaw, Z., Sepich, D.S., Johnson, A.N., Mokalled, M., Solnica-Krezel, L., Dobbs, M.B., and Gurnett, C.A. (2020). MYH3-associated distal arthrogryposis zebrafish model is normalized with para-aminoblebbistatin. *EMBO Mol Med* 12**,** e12356.

Wise, C.A., Gao, X., Shoemaker, S., Gordon, D., and Herring, J.A. (2008). Understanding genetic factors in idiopathic scoliosis, a complex disease of childhood. *Curr Genomics* 9**,** 51-59.

Wu, Z., Zhu, X., Xu, L., Liu, Z., Feng, Z., Hung, V.W.Y., Cheng, J.C.Y., Qiu, Y., Lee, W.Y.W., Lam, T.P., and Zhu, Z. (2023). More Prevalent and Severe Low Bone-Mineral Density

in Boys with Severe Adolescent Idiopathic Scoliosis Than Girls: A Retrospective Study of 798 Surgical Patients. *J Clin Med* 12.

Xie, H., Li, M., Kang, Y., Zhang, J., and Zhao, C. (2022). Zebrafish: an important model for understanding scoliosis. *Cell Mol Life Sci* 79**,** 506.

Zhang, X., Jia, S., Chen, Z., Chong, Y.L., Xie, H., Feng, D., Wu, X., Song, D.Z., Roy, S., and Zhao, C. (2018). Cilia-driven cerebrospinal fluid flow directs expression of urotensin neuropeptides to straighten the vertebrate body axis. *Nat Genet* 50**,** 1666-1673.

Zhou, T., Gao, B., Fan, Y., Liu, Y., Feng, S., Cong, Q., Zhang, X., Zhou, Y., Yadav, P.S., Lin, J., Wu, N., Zhao, L., Huang, D., Zhou, S., Su, P., and Yang, Y. (2020). Piezo1/2 mediate mechanotransduction essential for bone formation through concerted activation of NFAT-YAP1-ß-catenin. *Elife* 9.

Zhu, D., Zhang, G., Guo, X., Wang, Y., Liu, M., and Kang, X. (2021). A New Hope in Spinal Degenerative Diseases: Piezo1. *Biomed Res Int* 2021**,** 6645193.

Achievement

Ramli., Toshihiro Aramaki, Masakatsu Watanabe, Shigeru Kondo. (2023). Piezo1 Mutant Zebrafish as a Model of Idiopathic Scoliosis. Front. Genet. Volume 14 - 2023 | doi: 10.3389/fgene.2023.1321379